Hydrocracking of Long Chain n-Paraffins under Fischer-Tropsch Conditions

Matthew A. Koen
Jack C.Q. Fletcher
Roald Brosius

Submitted in partial fulfilment of the requirements
of the degree of Master of Science in Chemical Engineering

August 2014

Center for Catalysis Research
Department of Chemical Engineering
University of Cape Town
Cape Town
South Africa

Acknowledgements

This dissertation would not be possible without the contributions of many supporting groups and individuals. The author would like to acknowledge and thank all involved in the completion of this project, specifically:

Dr Roald Brosius for his time, assistance, dedication and helpful insight without which this project would not have been possible

Professor Jack Fletcher for providing focus and much needed instruction on the direction of the project

Mr Dirk Reyskens for his help and patience in the laboratory

UCT Chemical Engineering Department and the Catalysis Research Centre for allowing the use of their laboratory equipment and resources

c*change for the financial support and guidance throughout the duration of the research

The National Research Foundation (NRF) for the financial assistance during this project. Opinions expressed and conclusions arrived at, are those of the author and are not necessarily to be attributed to the NRF.

Declaration

I, the undersigned, hereby certify that this dissertation contains work that is my own research and interpretation completed with the assistance of my supervisors (indicated in the Acknowledgements). Any information which is not my own has been indicated as such and referenced in accordance with the Harvard-UCT referencing system.

Signed: _____

Name: _____

Date: _____

Synopsis

A number of various iron-palladium loaded H-MFI zeolites used for the hydrocracking of n-hexadecane under Fischer-Tropsch conditions were tested to address the inherent low CO tolerance of the pure palladium noble metal hydrocracking catalysts. The hydrocracking mechanism consists of two functions, namely the metal de-/hydrogenation (HD/DHD) and the acidic β-scission function. The addition of CO to reactions involving monometallic palladium hydrocracking catalysts has led to an imbalance between these functions due to the migration of the noble metal resulting in significant and undesirable secondary cracking. However, the inclusion of iron to the hydrocracking catalyst may allow for chemical anchoring of the noble metal (Wen et al., 2002) reducing the effect of the migration and thus retaining the bifunctional balance. The consequent palladium-iron alloy (Garten, 1976) also has the potential for an improved rate of de-/hydrogenation (Fukuoka et al., 1990) resulting in a greater rate of intermediary carbenium ions which in turn could lower any undesired secondary cracking reactions already present.

The Fe/H-MFI precursor was prepared using a solid-state ion exchange after which incipient wetness impregnation was used to add the palladium. Different loadings of palladium and iron were used to prepare the PdFe/H-MFI catalysts in order to determine an optimum ratio loading. All experiments were conducted at standard low temperature Fischer-Tropsch conditions in a plug-flow fixed trickle-bed reactor equipped with a homogeneously operating evaporator and on-line GC-FID analysis.

It was found that none of the bimetallic catalysts produced showed any greater tolerance to carbon monoxide when compared to the monometallic catalyst. The results indicated that the behaviour of the bimetallic catalyst was near identical to that of the monometallic catalyst in the presence of CO. It was thus concluded that the preparation method used, in particular the Fe/H-MFI precursor through solid state ion-exchange, was unsuitable for the production of an alloyed PdFe/H-MFI catalyst.

An effect of iron was noted in the low palladium high iron loaded catalyst i.e. PdFe/H-MFI (16,12). In the absence of CO, this catalyst showed a significantly improved selectivity when compared to the low palladium low iron catalyst, PdFe/H-MFI (16,24). This effect of iron was attributed to the blockage of the H-MFI pores due to the large amount of iron present. As a consequence of this, access to the internal acid sites is severely limited and therefore are essentially removed from the hydrocracking reaction. As such the PdFe/H-MFI (16,12) has an improved metal:acid site balance.

Poisoning by water (a Fisher-Tropsch product) was found to significantly reduce secondary cracking due to deactivation of the acid sites (lowering of total acidity) resulting in improved selectivity through intermediary olefin product promotion. From this, almost pure primary cracking was possible allowing the noble metal catalysts to retain its ideal hydrocracking properties at very high conversions (as evident by the high isomerization selectivity). This indicates that if the total acid strength of the H-MFI zeolite could be reduced (e.g. dealumination), the overall catalyst selectivity could be improved.

Testing into whether the effect of water in reducing secondary cracking could be used to offset the effect of an increase in secondary cracking by CO addition, proved ineffective. It is therefore thought that CO not only causes palladium migration and clustering on the external zeolite but also poisons the active metal sites still available. As a result the balance between the metal and acid function could not be restored.

It is thus recommended that for future work a zeolite with a lower total acid strength be used in conjunction with a alternate method for iron addition. Furthermore, testing into higher loadings of palladium may prove fruitful in balancing its migratory nature in the presence of carbon monoxide.

Table of Contents

Synopsis i

List of Figures v

List of Tables vii

1 Introduction 1

2 Background 3

2.1 Global Energy and Fossil Fuels . . . 3
2.1.1 Transport Fuel Production from Oil . . . 3
2.1.2 Gas-to-Liquid and Coal-to-Liquid Technology . . . 6
2.1.2.1 A Brief History . . . 6
2.1.2.2 The Fischer-Tropsch Process . . . 6
2.1.2.3 High Temperature and Low Temperature Fischer-Tropsch . . . 6
2.1.2.4 Anderson-Schulz-Flory Product Distribution . . . 7
2.2 Types of Hydrocracking . . . 9
2.2.1 Conventional Hydrocracking . . . 9
2.2.2 Mild Hydrocracking . . . 9
2.2.3 Fischer-Tropsch Wax Hydrocracking . . . 10
2.3 Bifunctional Hydrocracking Catalysts . . . 11
2.3.1 Hydrocracking Mechanisms . . . 11
2.3.1.1 Classification of β-scission reactions . . . 11
2.3.2 Ideal Hydrocracking . . . 13
2.3.3 Non-Ideal Hydrocracking and the Factors Affecting Hydrocracking Catalyst Ideality . . . 13
2.4 Selection of Palladium Metal Function . . . 14
2.5 Iron addition to Supported Palladium Catalysts . . . 14
2.5.1 Rate of Dehydrogenation/Hydrogenation . . . 14
2.5.2 Chemical Anchoring of Palladium . . . 15
2.5.3 Pd-Fe Alloy Formation . . . 15
2.6 Zeolites . . . 16
2.6.1 Effect of Zeolite Selection on Hydrocracking Selectivity . . . 16
2.6.1.1 H-MFI Zeolite . . . 17
2.6.2 Hydroisomerization . . . 18
2.6.3 Interdependence of Selectivity and Conversion . . . 18

3 Research Objectives 21

3.1 Hypothesis . . . 21
3.2 Key Questions . . . 21
3.3 Scope and Limitations . . . 22

4 Experimental **23**
4.1 Catalysts . . . 23
4.1.1 Palladium-Iron Naming Convention . . . 23
4.1.2 Various Catalysts Tested . . . 23
4.1.3 Catalyst Preparation . . . 24
4.2 Catalyst Testing . . . 24
4.2.1 Hydrocracking Test Apparatus . . . 24
4.2.1.1 Test Unit Auxiliary Components . . . 24
4.2.2 Catalyst Pretreatment . . . 27
4.2.2.1 Reactor Loading . . . 29
4.2.2.2 Calcination . . . 29
4.2.2.3 Reduction . . . 29
4.3 Test Procedure . . . 29
4.3.1 Start-up Procedure . . . 29
4.3.2 On-line Procedure . . . 30
4.3.2.1 Temperature . . . 30
4.3.2.2 Water Addition/Removal . . . 30
4.3.2.3 CO Addition/Removal . . . 30
4.3.3 Shut-down Procedure . . . 31
4.4 Gas Analysis . . . 31
4.4.1 Gas Chromatography . . . 31
4.4.2 Sampling Procedure . . . 31
4.4.3 Analysis Conditions . . . 32
4.5 Data Work-up . . . 32

5 Experimental Results and Analyses **33**
5.1 Base Case Results of Monometallic Pd/H-MFI . . . 33
5.1.1 Defining Reference Ideality for Catalyst Comparison . . . 33
5.1.2 Effect of Carbon Monoxide on Pd/H-MFI Hydrocracking Selectivity . . . 36
5.2 Results of Bimetallic PdFe/H-MFI Catalyst Tested . . . 36
5.2.1 Effect of Low Iron Loading on Selectivity and Conversion . . . 36
5.2.2 Effect of High Iron Loading on Selectivity and Conversion . . . 38
5.2.3 Effect of Palladium Loading on Selectivity and Conversion . . . 41
5.2.4 Effect of Water on PdFe/H-MFI Catalysts . . . 42
5.2.5 Carbon Monoxide Tolerance of PdFe/H-MFI Catalysts . . . 44

6 Discussion **45**
6.1 Effect of Iron and Palladium Loading on PdFe/H-MFI Catalyst . . . 45
6.2 Effect of Water on PdFe/H-MFI Catalyst . . . 46
6.3 Carbon Monoxide Tolerance of PdFe/H-MFI Catalysts . . . 46

7 Conclusions and Recommendations **47**
7.1 Suitability of Bimetallic PdFe/H-MFI for Hydrocracking at Low Temperature Fischer-Tropsch Conditions . . . 47

References **49**

Appendix A Temperature Profiles **53**

Appendix B Nitrogen Dilution **57**

List of Figures

2.1 Simplified flow diagram of a complex refinery by Owen and Coley (1995). 5
2.2 Fischer-Tropsch Synthesis stepwise product formation adapted from Bouchy et al. (2009); Dry (2001) 8
2.3 The Anderson-Schulz-Flory polymerization kinetics for hydrocarbon selectivity (weight fraction) as a function of the chain growth probability (α) - adapted from Kukard (2008) 8
2.4 Bifunctional hydrocracking and hydroisomerization mechanism for long chain n-paraffins adapted from Bouchy et al. (2009). 11
2.5 Classification of β-scission reactions of alkylcarbenium ions (where i = number of carbons in hydrocarbon molecule) by Weitkamp (2012). 12
2.6 Correlation between activity in n-hexadecane hydrocracking and metal loading re-drawn from Brosius and Fletcher (2013). 15
2.7 Ball and stick representation of the H-MFI zeolite structure showing the pore channel between unit cells (Baerlocher and McCusker, 2013). 17
2.8 Representation of the intersection of sinusoidal and straight pore channels in H-MFI zeolite (Baerlocher and McCusker, 2013). 17
2.9 Molar carbon number product distribution for the hydrocracking of of n-C_{16} adapted from (Bouchy et al., 2009; Weitkamp, 2012). 19
2.10 Representation of Conversion vs Yield for cracking of long chained n-paraffins over a bifunctional catalyst, adapted from Martens and Jacobs (2001). 19

4.1 Process flow diagram of hydrocracking test unit. 25
4.2 Schematic of on-line hydrocracking sampling system. 26
4.3 Schematic of reactor head showing the entrance pathways of the feed components allowing for homogeneous mixing in the gas phase. 28
4.4 Schematic of Guard Pot under normal flow conditions (left) and abnormal (reverse flow) conditions (right) showing the liquid condensation in the pot. 28

5.1 Graph of the overall conversion of feed n-hexadecane at various temperatures as a function of the sample run number over the base case 0.96 wt% Pd/H-MFI catalyst. 34
5.2 Graph of the selectivity of base case 0.96 wt% Pd/H-MFI catalyst at 215 °C and a overall n-hexadecane conversion of 16%. 34
5.3 Graph of the selectivity of base case 0.96 wt% Pd/H-MFI catalyst at 240 °C and a overall n-hexadecane conversion of 91%. 35
5.4 Graph of the C_4/C_{12} mass fractions as a function of overall n-hexadecane conversion for the monometallic Pd/H-MFI catalyst. 35
5.5 Graph of the selectivity in the presence of carbon monoxide of base case 0.96 wt% Pd/H-MFI catalyst at 225 °C and a overall n-hexadecane conversion of 40%. 36
5.6 Graph of the selectivity of base case 0.96 wt% Pd/H-MFI catalyst at 230 °C and a overall n-hexadecane conversion of 40%. 37
5.7 Comparison of the C_4/C_{12} mass fractions as a function of overall n-hexadecane conversion for the monometallic Pd/H-MFI and bimetallic PdFe/H-MFI (4,24) catalysts. 37

5.8 Correlation between total carbon fraction selectivities of 0.96 wt% Pd/H-MFI with various iron loadings at 215-225°C and an overall n-hexadecane conversion of circa 30%. 39
5.9 Comparison of the C_4/C_{12} mass fractions as a function of overall n-hexadecane conversion for the monometallic Pd/H-MFI and bimetallic PdFe/H-MFI (16,12) catalysts. 39
5.10 Graph of the selectivity of base case 0.96 wt% Pd/H-MFI catalyst at 225 °C and a overall n-hexadecane conversion of 30%. 40
5.11 Graph of the selectivity of PdFe/H-MFI (4,12) catalyst at 225 °C and a overall n-hexadecane conversion of 31%. 40
5.12 Graph of the C_4/C_{12} mass fractions for 0.96 wt% and 0.16 wt% palladium loaded catalyst as a function of overall n-hexadecane conversion. 41
5.13 Graph of the conversion and selectivity towards feed isomerization mass fraction for 0.96 wt% palladium loaded catalyst as a function of reaction temperature. 42
5.14 Graph of the selectivity of PdFe/H-MFI (4,24) catalyst at an overall n-hexadecane conversion of 24%. 43
5.15 Graph of the selectivity of PdFe/H-MFI (4,24) catalyst at an overall n-hexadecane conversion of 22% in the presence of H_2O. 43
5.16 Overall selectivity of the monometallic Pd/H-MFI and various bimetallic PdFe/H-MFI catalysts in the presence of CO after approximately 24 hours. 44

A.1 Reactor 1 isothermal temperature zone with error band. 55
A.2 Reactor 2 isothermal temperature zone with error band. 55

B.1 Reactor 1 N_2 dilution flow rate inlet capillary pressure calibration graph. 58
B.2 Reactor 1 N_2 dilution flow rate inlet capillary pressure calibration graph. 58

List of Tables

2.1 Property variation of different crude oils, extracted from Speight and Ozum (2001). Approximate physical composition in weight percent 4
2.2 Fractions of crude oil derived distillate transport fuels, modified from Goodger (2001) 4
2.3 Hydrocracking products from various process feedstocks (Scherzer and Gruia, 1996) . 9
2.4 Typical process conditions of hydrotreating and various hydrocracking processes (Bouchy et al., 2009; Scherzer and Gruia, 1996; Speight and Ozum, 2001; Tasaka et al., 2012) 10
2.5 General summary of various zeolite structure types and their industrial uses Hagen (1999) 16

4.1 Specifications for the preparation of the various hydrocracking catalysts tested. . . . 23
4.2 Gas chromatography column oven program conditions for reactor product analysis. . 32

A.1 Heating block set point temperatures used to determine isothermal reactor zone. . . 54
A.2 Individual reactor isothermal temperatures. 54
A.3 Heating block set points for a desired reactor temperature of 225 °C 54

Chapter 1
Introduction

"The higher the mountain, the more treacherous the path."
Francis Underwood - House of Cards

Project Background

According to the BP Statistical Review 2013 (BP, 2013), the global energy consumption continues to increase and will do so for the foreseeable future. While oil continues to have the majority share of the energy market, its growth rate is slower than that of both coal and natural gas. Growth in energy consumption of developing countries such as South Africa increased by 30% over the last ten years indicating that industrial energy security is becoming increasingly important.

Within this, the security and sustainability of middle distillate fuel production (such as diesel) is a major component in the petrochemical industry as it is used in both passenger and commercial vehicles. The low temperature Fischer-Tropsch (LTFT) synthesis of middle distillate fuels is a proven commercial process in which high quality diesel is made. Currently this process comprises of three key steps. Fossil fuel (coal or natural gas) is converted into syngas (carbon monoxide and hydrogen) before being reacted to produce long-chained hydrocarbon wax. This wax is then subsequently cracked in the presence of hydrogen to produce the desired diesel product. It was found that under mild hydrocracking conditions (typically 623–690 K, 60-150 bar (Ray Chaudhuri et al., 1995; Valavarasu et al., 2003)) this process can produce an overall diesel yield of 80% with the cetane number of the hydrocracked diesel being 65 (due to branched paraffins), which is comparable to the straight-run LTFT diesel cetane number of 75. The combination of straight-run Fischer-Tropsch diesel and hydrocracked diesel provides the improved cold flow properties needed for its use in transportation while maintaining a relatively high cetane number (Bouchy et al., 2009; Dry, 1990).

Hydrocracking catalysts are well known to consist of two functions and have been extensively reviewed citepbouchy2009fischer,choudhary1975hydrocracking,weitkamp2012catalytic. These functions include a metal hydrogenation and dehydrogenation (HD/DHD) function and an acid cracking function. The metal function can be provided by a transition (group VIII) or noble metal and the acidic function by a zeolite or amorphous silica-alumina support (Leckel and Liwanga-Ehumbu, 2006; Speight and Ozum, 2001).Current hydrocracking catalysts such as nickel (5% by weight) on silica-alumina operate effectively at 350-370 °C and 100 bar (Speight and Ozum, 2001); well above the normal LTFT reaction conditions of 225 °C and 26 bar for fixed bed reactors (Dry, 1996). It is of particular interest to obtain a catalyst that performs comparable to commercial catalysts at the LTFT conditions in order to avoid harsh conditions and eventually obtain integration of the Fischer-Tropsch reaction and wax hydrocracking steps.

Noble metals such as palladium and platinum may be used as the active hydrogenating components of the hydrocracking catalyst. These metals favour higher boiling point product formation (middle distillate products) over their transition metal counterparts such as nickel and molybdenum (Choudhary and Saraf, 1975). They are however unsuitable for most industrial applications due to the presence of sulphur, oxygen and nitrogen compounds in the feedstock (Speight and Ozum,

2001; Valavarasu et al., 2003). Dry (2001) however listed the essentially insignificant amount of sulphur, nitrogen compounds in Fischer-Tropsch wax as one of the reasons for the processes ability to produce high quality diesel. This, in conjunction with the fact that noble metals are active at LTFT conditions (Weitkamp et al., 1983; Elangovan et al., 2002), make them an ideal candidate for process integration.

Previous work by Brosius and Fletcher (2013) has shown that platinum and palladium are ideal hydrocracking catalysts under the LTFT operating conditions but that platinum is irreversibly and totally deactivated by the presence of carbon monoxide - a component of the LTFT reaction feed. The tested palladium catalyst however shows only partial deactivation but a complete transformation to non-ideality indicated by a significant increase in secondary cracking and low carbon number production. This shift towards non-ideality has been attributed to the migration of the highly mobile Pd^{2+} ion (Wen et al., 2002). Consequently, the removal of active metal Pd sites causes the elimination of the metal-acid quasi-equilibrium resulting in over-cracking and a poor product spectrum.

Studies into chemical anchoring of noble metals into zeolite pores provide a promising solution to the migration of noble metals (Tzou et al., 1986; Wen et al., 2002). In particular, the use of iron (Fe ions and/or Fe-oxo ions) has been found to effectively anchor palladium inside the ZSM-5 zeolite as well as improve palladium particle dispersion and nucleation and reduce particle growth (Fukuoka et al., 1990; Garten, 1976; Wen et al., 2002). It has also been seen that water, a product of the LTFT reaction, has a promotional hydrocracking effect due its ability to hydrate the protons present thus deactivating the catalyst by diminishing acid strength (Yan, 1972).

With this in mind, there exists a possibility of chemically anchoring palladium inside the zeolite pores as well as alleviating the affects of any additional migration with the addition of water thus restoring the metal-acid balance. In doing so the retention of the ideality of the Pd-Zeolite hydrocracking catalyst may be achievable.

Hypothesis

It is thus hypothesized that there exists an opportunity to synthesize CO tolerant palladium-iron catalysts for Fischer-Tropsch wax hydrocracking. It is believed that addition of Fe to Pd/Zeolite catalysts will prevent the migration of Pd (upon the co-feeding of CO) to the external surface and act as a chemical anchor through strong d-orbital interactions.

Furthermore it is theorized that due to these Pd-Fe interactions that the addition of Fe to Pd/Zeolite catalysts will weaken the Pd-CO chemical bond by changing the metal electron density thus reducing poisoning of the catalysts. This in conjunction with the addition of water, will likely result in an active, CO tolerant and middle distillate selective hydrocracking catalyst.

Key Questions

The focus of this project will be on the performance of the prepared catalyst in terms of both activity and selectivity towards middle distillate products. In order to achieve this, this study will focus on key aspects including the effect of:

- iron loading on the CO tolerance of the bimetallic Pd-Fe catalysts as compared to the monometallic Pd catalyst
- the addition of water to the bimetallic and monometallic catalysts

These aspects will be evaluated by testing and comparing the hydrocracking activity and selectivity of various Pd-Fe ratios on a zeolite support in the presence of CO and water.

Chapter 2
Background

"Dude, sucking at something is the first step towards being sorta good at something."
Jake the Dog - Adventure Time

2.1 Global Energy and Fossil Fuels

Note: Portions of this review have been adapted from a literature study by Koen and Manan (2012).

The total global energy consumption relies heavily on fossil fuels. While renewable energy (wind, solar) and hydroelectric power has shown significant growth, it still only accounts for a combined 9% of the total global energy output (BP, 2013). Oil (33%), coal (30%) and natural gas (24%) account for the majority of the global energy supply with nuclear power providing the balance (4%). The use of oil is however decreasing globally due to the increased consumption of coal and natural gas. It is forecast that by 2035 the use of fossil fuels will still account for over 80% of the global demand based on current trends with oil, natural gas and coal contributing roughly the same amount resulting in no single dominant fuel (BP, 2014). These trends indicate that research into the efficient production of transportation fuels from fossil fuels, in particular coal and natural gas, is relevant for future sustainability.

2.1.1 Transport Fuel Production from Oil

Conventional transportation fuels (petrol, diesel and aviation fuel) are mainly produced through the distillation of crude oil (sometimes referred to a petroleum) which contains a mixture of hydrocarbons not least of which are paraffins, olefins, naphthalenes and aromatics. The composition of crude oil varies significantly with origin and therefore exhibits different properties (see table 2.1). In this process the liquid fuels are separated into fractions based on their boiling points. With the inclusion of auxiliary units, between 30 and 70% of all the crude oil processed may be converted to gasoline and diesel fuels (Owen and Coley, 1995). Table 2.2 shows the typical ranges of the various transportation fuel fractions in crude oil distillation.

The process of transportation fuel production through petroleum distillation begins with preliminary treatment to remove unwanted materials (e.g. salt). It is then preheated before being sent to an atmospheric distillation column. The crude oil is kept at below 350 °C to ensure minimal decomposition due to thermal cracking (Speight and Ozum, 2001) while various fractions are then distilled off as 'straight run products'. Modern day refineries include a number of ancillary units for the fuel upgrading. These treatment and conversion units include catalytic reforming and isomerization (used for octane upgrading), mercaptan oxidation (conversion of mercaptans to disulfides), hydrotreating (hydrodesulfurization) and alkylation of light gases. The residual heavy components of the crude oil feed (referred to as residuum) may then be processed by a vacuum distillation column before being converted through thermal cracking, visbreaking and catalytic cracking. A simplified flow diagram of an oil refinery can be seen in figure 2.1 on page 5.

Table 2.1: Property variation of different crude oils, extracted from Speight and Ozum (2001). Approximate physical composition in weight percent

Origin	Specific gravity (Water=1.000)	Gasoline BP <205 (°C)	Kerosene BP=205-290 (°C)	Gas Oil BP=290-600 (°C)	Residuum BP >600 (°C)
Texas	0.864	44.9	4.2	23.2	27.9
Iraq	0.844	45.3	15.7	15.2	23.8
Iran	0.836	45.1	11.5	22.6	20.8
Kuwait	0.860	39.2	8.3	20.6	31.9
Bahrain	0.861	26.1	13.4	34.1	26.4
Saudi Arabia	0.840	34.5	8.7	29.3	27.5
Venezuela	0.895	15.3	7.4	77.3	-

Table 2.2: Fractions of crude oil derived distillate transport fuels, modified from Goodger (2001)

Technical Name	Distillation Temp. Range (°C)	Density (kg/L)	Hydrocarbon Range	Engine Application
Aviation Fuel	40 - 153	0.72	C_5-C_{10}	Spark-ignition piston (S-I)
Petrol	25 - 190	0.75	C_5-C_{10}	Spark-ignition piston (S-I)
Kerosene	152 - 256	0.80	C_9-C_{14}	Gas Turbine (GT)
Auto Diesel	165 - 350	0.84	C_{10}-C_{22}	High Speed Compression ignition piston (C-I)
Diesel Fuel	200+	0.86	C_{12+}	Low Speed Compression ignition piston (C-I)

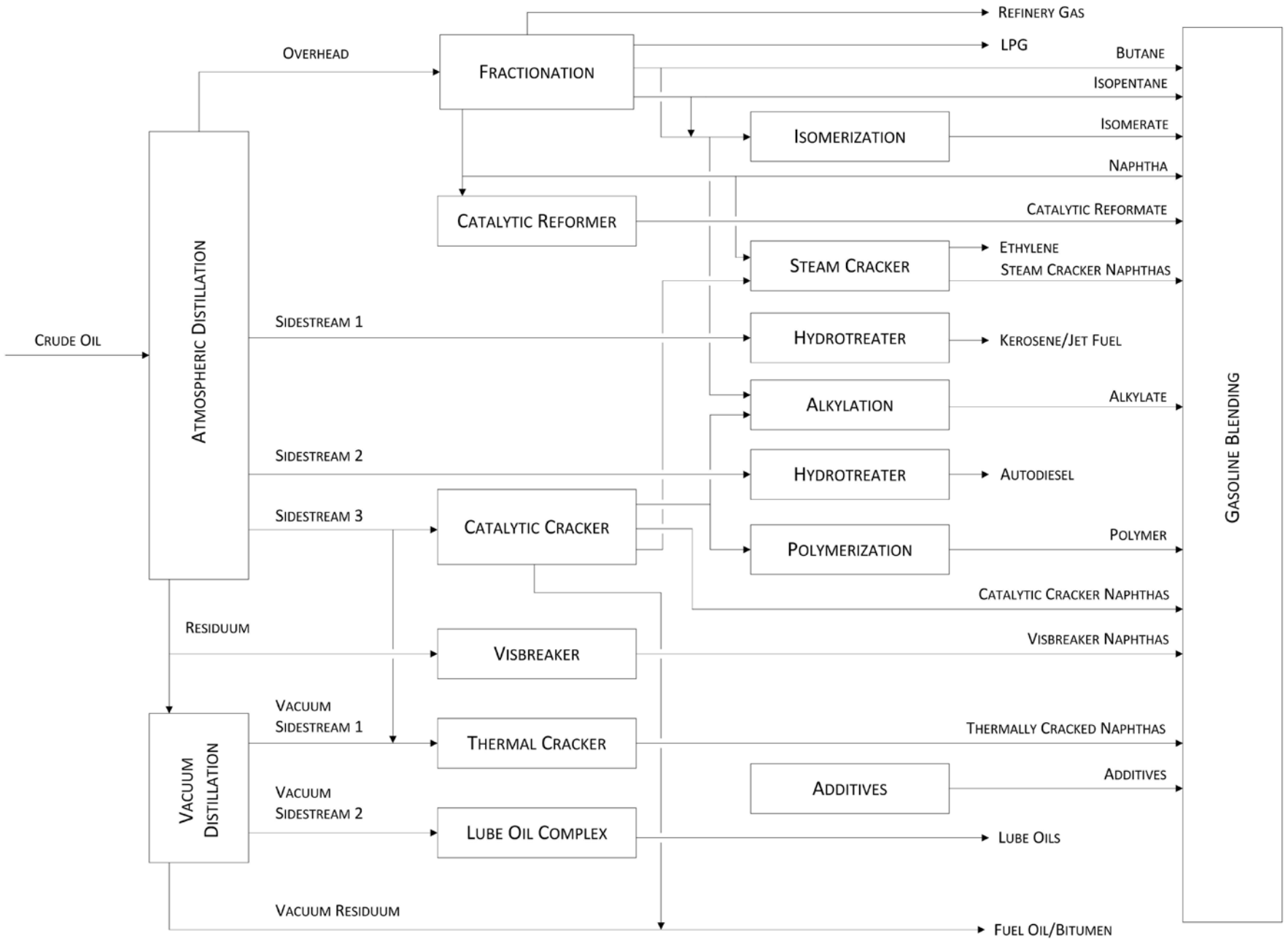

Figure 2.1: Simplified flow diagram of a complex refinery by Owen and Coley (1995).

2.1.2 Gas-to-Liquid and Coal-to-Liquid Technology

2.1.2.1 A Brief History

The development of one of the most influential coal-to-liquid technologies, now known as Fischer-Tropsch synthesis (FTS), was first introduced by Frans Fischer and Hans Tropsch in mid-1920 at the Kaiser Wilhelm Institute for Coal Research (now the Max Plank Institute) in Mülheim/Ruhr, Germany. The industrial application of the technology first became apparent in Germany 1938 and peaked during World War II.

The economic viability of the fuel derived from the Fischer-Tropsch process is highly dependent on the oil-price and the availability of crude oil. Thus, due to the discovery of large oil fields in the Middle East in 1955-1970, the interest in Fischer-Tropsch synthesis declined – with the exception being the South African industry at Sasol, Sasolburg due to the availability of cheap domestic coal and the political policy (Dry, 2002; Schulz, 1999).

In the early 1970s the oil price was approximately US$10 but had risen to approximately US$30 by 1980. This significantly improved the commercial viability of the Fischer-Tropsch process and Sasol built two more plants in Secunda, South Africa which ensured a combined coal-to-liquid (CTL) plant capacity of 7500 kilotonnes per annum (Dry, 2001). In the early 1990s, gas-to-liquid plants owned by Mossgas (presently PetroSA) in Mossel Bay, South Africa and Shell in Bintulu, Malaysia were built with a capacity of 1 000 kilotonnes and 500 kilotonnes per annum respectively (Dry, 2002). This was however accompanied by a decrease in the oil price to US$ 10 per barrel. Since the mid-1990s however, the oil price has increased dramatically and, adjusting for inflation, averaged around US$ 90 in 2013 which has made the production of fuel via FTS extremely profitable.

In 2007, the first international commercial gas-to-liquid FTS plant (Oryx GTL) was commissioned through a joint venture between Sasol and Qatar Petroleum with a capacity of 32,400 barrels per day (1 600 kilotonnes per annum) (Sasol, 2013). Currently, the world's largest GTL plant (Pearl GTL) is situated in Ras Laffan, Qatar and is owned by Shell. It has a capacity of 260,000 barrels per day (approximately 13 000 kilotonnes per annum) of GTL products and natural gas liquids per day and accounts for almost 8 % of Shell's total production output (Shell, 2014).

2.1.2.2 The Fischer-Tropsch Process

The Fischer-Tropsch reaction is a commercially proven process whereby coal is initially gasified to produce carbon monoxide and hydrogen (synthesis gas or 'syngas') before being sent to the Fischer-Tropsch reactor in which the FTS polymerization reaction occurs. This polymerization reaction uses -CH_2- as a monomer to produce hydrocarbon synthetic fuels (light petroleum gases to heavy fuel oils) as well as long-chain waxes. The process of producing syngas for FTS may also be done using natural gas as a feed source through steam reforming. In this case natural gas is reacted with steam before being sent to the Fischer-Tropsch reactor.

2.1.2.3 High Temperature and Low Temperature Fischer-Tropsch

Dry (2002) stated that syngas production accounts for approximately 60-70% of the plant capital and running cost and thus it can be seen as the most important factor in FTS. The full utilization of the retractables (CO, CO_2 and H_2) in the FT reactor and product upgrading is important to obtain maximum efficiency of the overall process (Dry, 2001).

The methods used to produce fuel via FTS are dependent on the natural feedstock available. High Temperature Fischer-Tropsch (HTFT) synthesis i.e. 340 °C and 20 bar (Dry, 2002), such as that used by the two Sasol plants in Secunda, South Africa use coal as the feed. The gasification of coal causes approximately 50% of the carbon feed to be converted to carbon dioxide which at high temperatures may be readily converted to carbon monoxide over iron-based catalysts via the water-gas shift (WGS) reaction shown equation 2.1.

$$H_2O + CO \leftrightarrow CO_2 + H_2 \tag{2.1}$$

In conjunction with the WGS reaction the overall FT synthesis, shown in equation 2.2, may convert all of the CO, CO_2 and H_2 feed gas into desirable products. This occurs at a $H_2/(2CO+3CO_2)$ ratio of 1.06 (Dry, 2002).

$$2.15H_2 + CO \leftrightarrow hydrocarbons + H_2O \tag{2.2}$$

The iron catalysts used are commonly promoted with an alkali substrate (e.g. 0.5 wt% K_2O) to maintain high activity and stability and requires a large tail gas recycle ratio (2:1) due to the conversion limitation caused by water production (Schulz, 1999). HTFT synthesis produces a variety of chemicals and favours the production of petrol as compared to diesel (Dry, 2001).

Low Temperature Fischer Tropsch (LTFT) synthesis, i.e. 230 °C and 27 bar (Dry, 2002), is favoured when natural gas is used as a feed source. The Shell Bintulu FT plant uses cobalt-based catalyst at these conditions to produce mainly wax and middle distillate products (Schulz, 1999). Cobalt based catalysts have a relatively low activity for the WGS reaction but are active for Fischer-Tropsch synthesis. Dry (2001) stated that due to the high hydrogen content of methane the carbon efficiency of methane reforming is higher than that of coal gasification making it the preferred raw material for middle distillate production. Schulz (1999) indicated that cobalt based catalyst do not suffer the same activity inhibition caused by water production as iron based catalyst and thus the conversion per pass may be higher. It was however stated that the selectivity using a cobalt based catalyst is strongly dependent on the partial pressures of CO and H_2 and that a sufficiently high CO partial pressure needs to be maintained throughout the reactor to ensure minimal CH_4 formation.

2.1.2.4 Anderson-Schulz-Flory Product Distribution

The need for wax hydrocracking is due to the product distribution obtained from the Fischer-Tropsch process. This product distribution follows the well-established Anderson-Schulz-Flory (ASF) kinetic theory irrespective of process conditions used and is based on the growth probability parameter, α. The ASF product distribution model is represented below in equation 2.3.

$$W_n = n \cdot (n - \alpha)^2 \cdot \alpha^{n-1} \tag{2.3}$$

In the above model, the parameter n is the number of carbons in the hydrocarbon molecule and the parameter W_n the mass fraction of the hydrocarbon molecule. The model follows a stepwise growth mechanism see figure 2.2. The mechanism described in figure 2.2 does not include the finer details of the exact chemical mechanism as many schemes have been postulated. The mechanism illustrates the growth of the hydrocarbon using a -CH_2- monomer as described by Dry (2001) and depicts the formation of alkanes as shown by Bouchy et al. (2009). Dry (2001) noted that at each step has the option of desorbing to produce alkenes or continue the chain growth process.

The value of α is dependent on a variety of factors including operating temperature; the type of catalyst used; catalyst promoters as well as the partial pressures of the reagents in contact with the catalyst. It was also stated that the value of α is mainly dependent on the ratio of the partial pressures of H_2 and CO in LTFT. Comparatively, in HTFT the total pressure of the system has a significant influence when using promoted catalysts while the influence of gas partial pressure of H_2, CO, CO_2 and H_2O is more complex.

Figure 2.3 shows that the ASF kinetic model limits the amount of transportation fuels that can be produced through FTS (gasoline and diesel) to approximately 40%. In order to increase the amount of fuel produced through FTS, current production mechanisms are geared towards maximum wax production and subsequent hydrocracking of the wax.

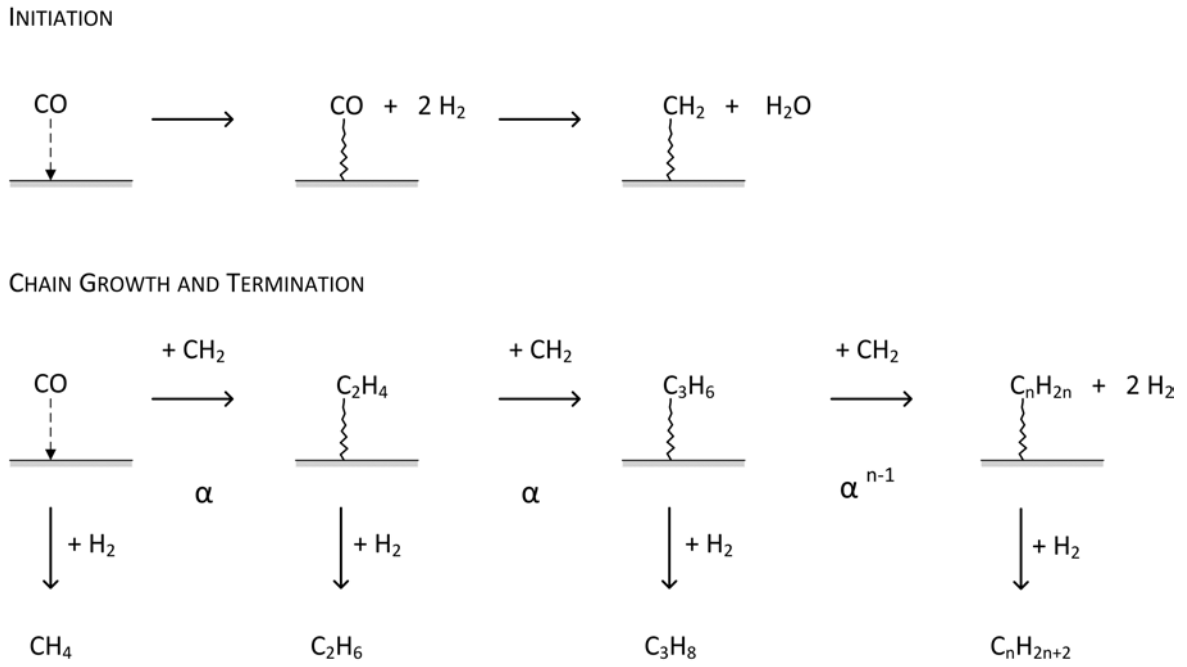

Figure 2.2: Fischer-Tropsch Synthesis stepwise product formation adapted from Bouchy et al. (2009); Dry (2001)

.

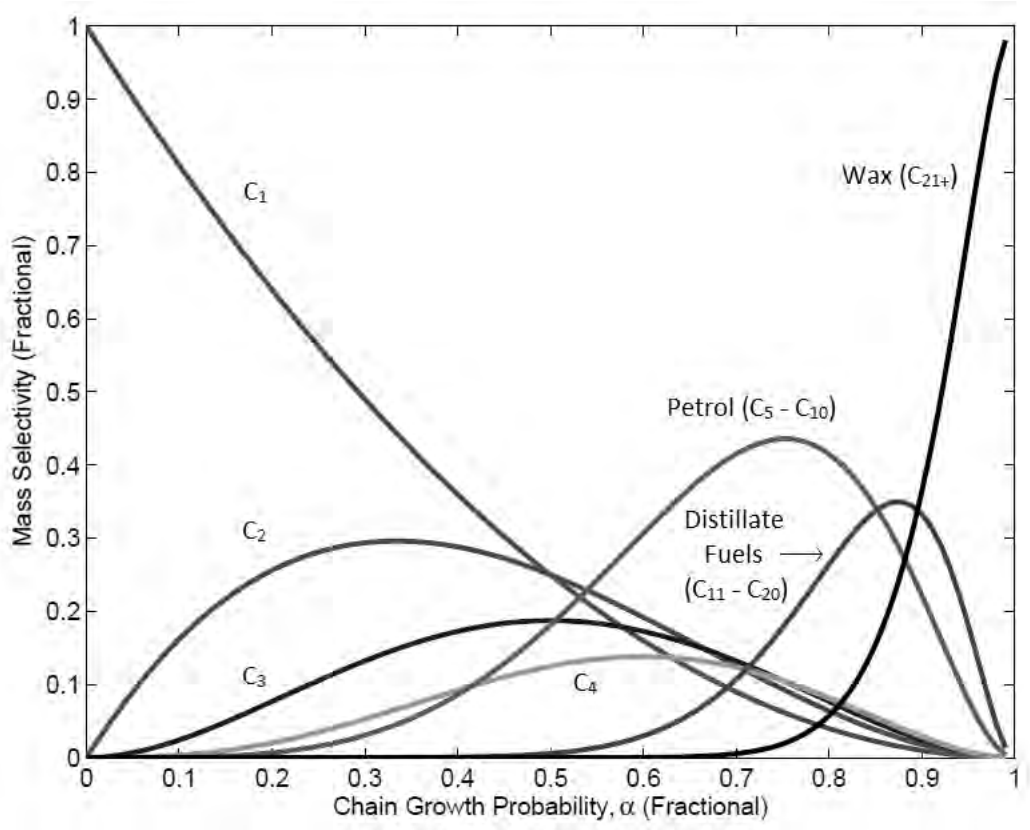

Figure 2.3: The Anderson-Schulz-Flory polymerization kinetics for hydrocarbon selectivity (weight fraction) as a function of the chain growth probability (α) - adapted from Kukard (2008)

.

2.2 Types of Hydrocracking

2.2.1 Conventional Hydrocracking

Modern hydrocracking has become an important and near indispensable refining process since its introduction in the 1960s due to the increased demands of transportation fuel and oils (Choudhary and Saraf, 1975; Scherzer and Gruia, 1996). One of its major advantages is the significant flexibility and versatility as it allows for the processing of a wide range of feedstocks into a wide range of products (Scherzer and Gruia, 1996; Weitkamp, 2012). This in turn allows the refinery to account for market fluctuations by producing a broad range of products in an existing unit as well as using different process variants (e.g. shape-selective, mild or conventional wax hydrocracking).

Conventional hydrocracking is mainly used for the production of transportation fuels from heavy crude oil fractions or vacuum gas oil (VGO) (Weitkamp, 2012). It can also be used for the upgrading of products from other units such as coker gas oil, deasphalted oil and fluid catalytic cracking (FCC) cycle oils (Scherzer and Gruia, 1996). The hydrocracking process removes long chain paraffins (dewaxing) in order to produce distillates and lube oils commonly of high quality. This high quality gasoline (research octane number(RON) of between 78 and 85) can then be used for blending with the gasoline pool. Similarly, diesel fuel with a relatively high cetane number (and low sulphur content) may be obtained through the hydrocracking process. Conventional hydrocracking usually takes place over a nickel-molybdenum or nickel-tungsten bimetallic catalyst supported on either an amorphous silica-aluminate or zeolite. The reaction conditions are usually in the range of 350-450 °C and an H_2 partial pressure of 85-140 bar (total pressure of 100-200 bar) resulting in various feedstock dependent products (Fahim et al., 2009; Scherzer and Gruia, 1996) - see table 2.3.

Table 2.3: Hydrocracking products from various process feedstocks (Scherzer and Gruia, 1996)

Feedstock	**Main Product**
Straight run gas oils	Light petroleum gas
Vacuum gas oils	Automobile gasoline
FCC gas oils	Reformer feedstock and jet fuel
Coker gas oils	Diesel fuels
Thermally cracked stock	Heating oils
Deasphalted oils	Olefin plant feedstock
Straight run and cracked naphthas	FCC feedstock

2.2.2 Mild Hydrocracking

Since the 1980s, the increase in demand for middle distillates for use in transportation, aviation, agriculture and industrial sectors has lead to the conversion of many refinery hydrotreaters into mild hydrocracking units (Ray Chaudhuri et al., 1995). Unlike the conventional hydrocracking units, mild hydrocracking operates at less severe conditions including a lower operating hydrogen partial pressure i.e. 35-70 bar (Fahim et al., 2009). This lower partial pressure of hydrogen leads to lower conversion (20-70%) and less hydrogenated products (Scherzer and Gruia, 1996). The conversion of existing units (such as a desulphurization hydrotreater) also results in a lower quality product due to the constraints of the existing equipment. However, owing to the high capital investment needed for conventional hydrocracking, the increase in overall conversion to middle distillates by the use of mild hydrocracking as a supplement offsets the lower product quality ensuring the economical viability of the process. The conditions of the process can be seen in table 2.4.

2.2.3 Fischer-Tropsch Wax Hydrocracking

In areas such as South Africa, where crude oil supplies are limited but coal is abundant, the use of the Fischer-Tropsch synthesis has been a commercially viable synthetic fuel production source despite the low efficiency of the process (Owen and Coley, 1995). The production of diesel through this process results in a high quality fuel with cetane numbers up to 75 consisting of mainly linear paraffins and virtually no sulphur, nitrogen or aromatic compounds (Dry, 2001; Bouchy et al., 2009).

The main aim of the hydrocracking stage of the Fischer-Tropsch process is to fulfil a number of key requirements. These requirements, as stated by Bouchy et al. (2009), include the ability of the catalyst to selectively convert heavy feedstock into middle distillates; the minimization of cracking of any middle distillates present in the feed as well as the selective isomerization of the middle distillates (feed and product) in order to improve the cold flow properties. Dry (2001) states that the best option for producing high quality diesel is to use a cobalt based catalyst in a slurry reactor; gearing the process for high wax production and then subsequently selectivity hydrocracking the wax to diesel fuel.

Catalysts used in FT wax hydrocracking are similar to that of conventional hydrocracking in that the metal function may be provided by noble metals (Pt or Pd) or transition metals sulphides (Ni-W, Ni-Mo, Co-Mo). The noble metal catalyst, albeit more expensive, can be seen as more active than that of their sulphide transition metal counterparts and are comparatively as effective due to the negligible amount of impurities in the FT wax feedstock (Bouchy et al., 2009). To ensure adequate production of middle distillates the acidic function must be the rate determining step (see section 2.3.2) and as such the minimization of mass transfer of olefinic compounds as well as the minimization of any confinement due to too strong adsorption should be considered when selecting acidic solids. As a result of this, large pore zeolites (such as Y zeolite) and low to medium acid strength silca-alumina based catalysts are more suited to middle distillate production (Bouchy et al., 2009) but have the effect of lowering the overall cetane number of the fuel.

The absence of sulphur and nitrogen compounds and the high chemical reactivity of heavy paraffin molecules allow high conversions of the FT feedstock to be obtained at mild hydrocracking conditions (Bouchy et al., 2009) see table 2.4.

Table 2.4: Typical process conditions of hydrotreating and various hydrocracking processes (Bouchy et al., 2009; Scherzer and Gruia, 1996; Speight and Ozum, 2001; Tasaka et al., 2012)

Operating Conditions	**Hydrotreating**	**Conventional hydrocracking**	**Mild hydrocracking**	**FT wax hydrocracking**
Conversion(%)	-	20-70	70-100	20-100
Total Pressure [bar]	75	100-200	50-80	35-70
H_2 pressure [bar]	25-50	85-140	35-70	10-50
Temperature [°C]	360-400	350-450	350-440	325-375
LHSV [h^{-1}]	0.5-2.5	0.5-2.0	0.3-1.5	0.5-3
		Catalyst		
Hydrogen Transfer	Co/Mo	Ni/Mo	Ni/Mo	Ni/W Ni/Mo
(Metal)	Ni/Mo	Ni/W Pd	Co/Mo	Pt Pd
Support	Alumina	Si-Al	Alumina	Si-Al
(Acid)	-	Zeolite	Si-Al	Zeolite

2.3 Bifunctional Hydrocracking Catalysts

2.3.1 Hydrocracking Mechanisms

The hydrocracking mechanism of n-paraffins has been extensively studied and is well understood to follow the β-scission (beta-scission) mechanism on a bifunctional catalyst (Bouchy et al., 2009; Scherzer and Gruia, 1996; Weitkamp, 2012). These catalysts, as the name suggests, contain two functions viz. a hydrogenation/dehydrogenation (HD/DHD) function provided by a metal and a Brönsted acidic function commonly provided by a zeolite. The mechanism is initiated via hydride extraction over the metal and the formation of an olefin compound. The olefin is then protonated at the acid site to form the carbenium ion. At this point an argument can be made for the inclusion of a propagation step in which intermolecular hydride transfer occurs (Weitkamp and Puppe, 1999) but is not included in the mechanism shown figure 2.4. Once the formation of the carbenium ion is completed, heterolytic bond cleavage at the beta position occurs. This results in the formation of a secondary carbenium ion and a smaller olefin. These smaller molecules are then deprotonated and hydrogenated (consuming the additional H_2) to give saturated compounds.

It is noted that the formation of stable tertiary carbenium ions can only occur with starting molecules containing eight or more carbon atoms. Bouchy et al. (2009) noted that the reaction of the molecules of this nature occurs much faster than the cracking of molecules with seven or less carbon atoms. As a result of this it is possible to obtain ideal hydrocracking catalysts in which the formation of light gases is almost negligible.

Figure 2.4 shows the generalized ideal hydrocracking mechanism proceeding via a tertiary carbenium ion, β-scission and protonation. The non-ideal case will result in the subsequent cracking of the second carbenium cation - known as secondary cracking. The possibility of secondary cracking is more prominent when there is an imbalance between the acidic function and the HD/DHD function which is often caused by poor metal distribution in zeolite supported catalysts.

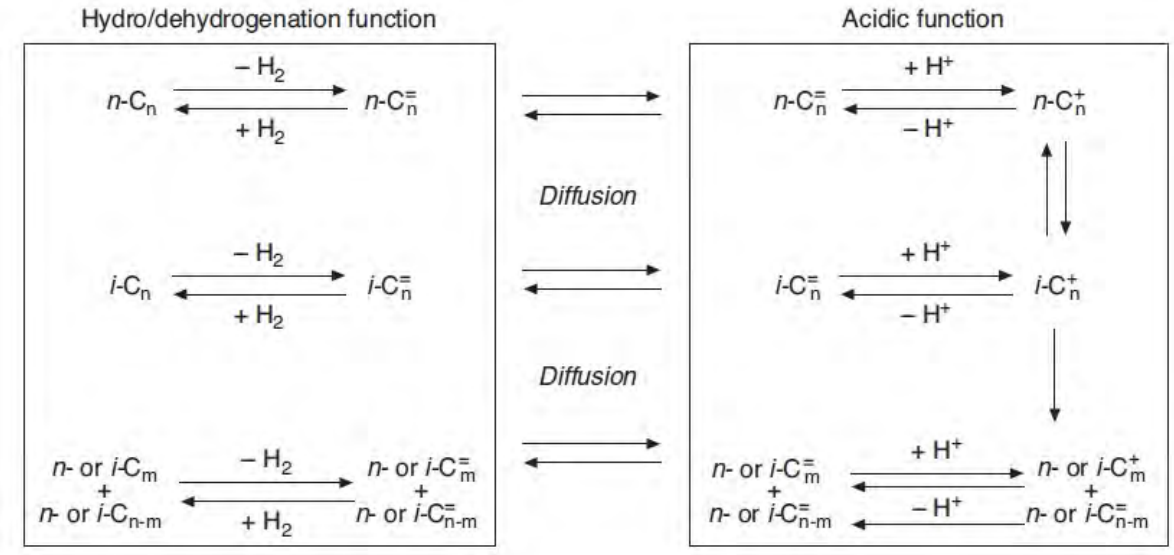

Figure 2.4: Bifunctional hydrocracking and hydroisomerization mechanism for long chain n-paraffins adapted from Bouchy et al. (2009).

2.3.1.1 Classification of β-scission reactions

As the rate controlling (and thus selectivity controlling) step of the hydrocracking mechanism relies on the acidic function it is important to understand the various hydroisomerization and β-scission

mechanisms available. The skeletal rearrangement of a hydrocarbon paraffin may occur through two separate avenues often referred to as Type A and Type B (Bouchy et al., 2009; Weitkamp, 2012).

In Type A hydroisomerization the change in the skeletal structure, i.e. a positional change of an alkyl branch, proceeds via an alkyl and hydride shift resulting in an unchanged degree of branching of the carbocation. Type B hydroisomerization however proceeds via the formation of a cyclic carbonium ion intermediated (e.g. protonated cyclopropane (PCP) mechanism) accompanied by an increase or decrease in the degree of branching. Weitkamp (2012) noted that Type A hydroisomerization is significantly faster than Type B. This results in a positional isomer fraction product distribution governed by the internal thermodynamic equlibria when using molecular non-shape selective bifunctional catalysts (Bouchy et al., 2009).

Similarly to the hydroisomerization step, the β-scission step may also be separated into various reaction types (see figure 2.5). Weitkamp (2012) showed that there are five types of β-scission with the following relative reaction rates In accordance with the stability of the carbocations involved:

$$\text{Type A} >> \text{Type B}_1 \approx \text{Type B}_2 > \text{Type C} >>> \text{Type D}$$

together with the two types of isomerization to show the relative rates that govern the overall hydrocracking mechanism (Weitkamp, 2012):

$$\text{Type A } \beta\text{-scission} > \text{Type A isomerization} > \text{Desorption} > \text{Type B isomerization} \approx \text{Type B}_1\ \beta\text{-scission} \approx \text{B}_2\ \beta\text{-scission} > \text{Type C } \beta\text{-scission} >> \text{Type D } \beta\text{-scission}$$

The fastest cracking reaction results from Type A and B β-scission reactions which both involve isomerized molecules. As a result of this, the hydrocracking of LTFT wax will inherently have the improved cold flow properties needed for middle distillates.

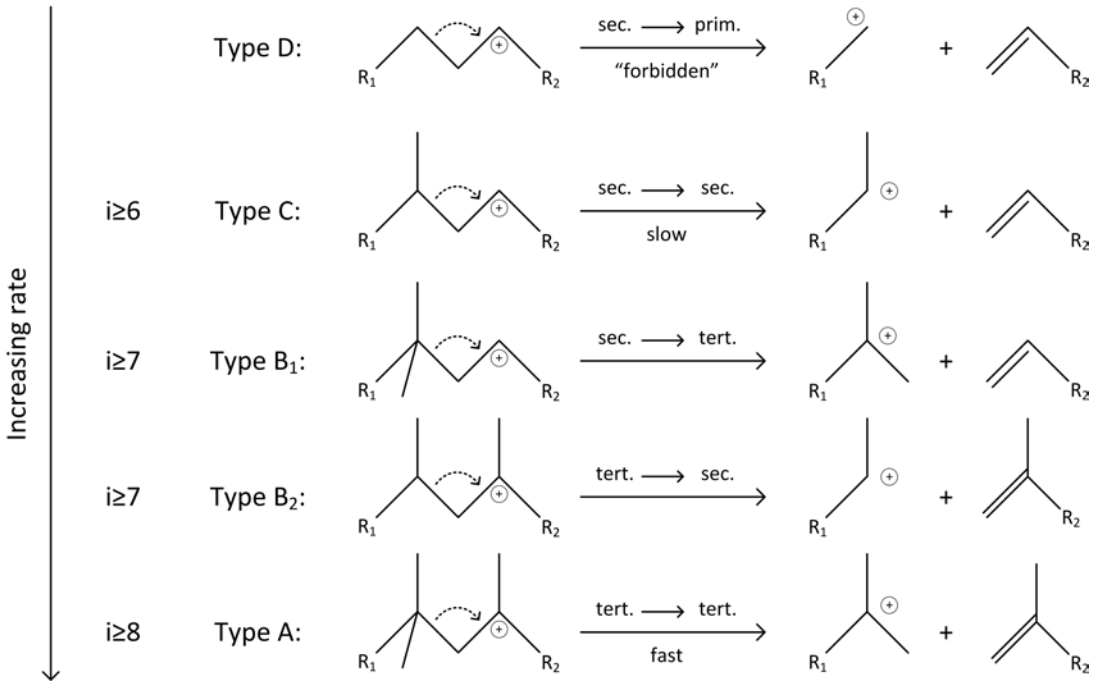

Figure 2.5: Classification of β-scission reactions of alkylcarbenium ions (where i = number of carbons in hydrocarbon molecule) by Weitkamp (2012).

2.3.2 Ideal Hydrocracking

The term "Ideal Hydrocracking" can be seen as a special case of bifunctional hydrocracking. As defined by Weitkamp (2012), in order for a catalyst to be termed ideal the following criteria must be met:

- the Wiesz-Prater intimacy criterion must be satisfied to ensure that the reaction rate is not limited by the transport of olefinic hydrocarbons i.e. the metal and acid sites need to be in close mutual proximity.
- the metal function (HD/DHD) should not be rate limiting and should balance the acid function by providing the maximum amount of intermediate olefins while quickly hydrogenating cracked olefin intermediates.

Catalysts that meet these requirements are considered to be ideal hydrocracking catalyst and have several prominent features. These features include:

- a low hydrocracking reaction temperature (c.a. 250 °C) as compared to that of catalytic cracking
- the allowance for a high selectivity of skeletal isomerization of long chain n-paraffins thereby producing high yields of iso-paraffins.
- the possibility of pure primary hydrocracking and a "flat" or "bell-shaped" carbon number product distribution.

The advantage of ideal hydrocracking catalysts are that they allow for maximum product yield; flexibility in a specific process and extreme versatility across the petrochemical refining spectrum. Under the conditions of ideal hydrocracking the production of middle distillates from LTFT may be maximized.

2.3.3 Non-Ideal Hydrocracking and the Factors Affecting Hydrocracking Catalyst Ideality

Conversely to the desired ideal hydrocracking system, catalysts may also present non-ideal behaviour. Like ideal catalysts they may also be defined by their salient features. Although any distribution not considered ideal may be termed non-ideal, common attributes among these catalyst are noticeable and the degree of non-ideality may be altered by a number of process conditions as stated by Thybaut et al. (2005). For a given ratio of acid to metal sites on a non-ideal catalyst in which the quasi-equilibrium of the HD/DHD and cracking functions is not present, the factors that lead to non-ideality include:

- a decreasing total pressure leading to the kinetic effect of increasing the carbenium ion concentration available for isomerization and cracking
- an increasing reaction temperature which leads to a moderate increase in the metal-catalysed reaction step but a large increase in the acid-catalysed reaction step resulting in more severe cracking
- an increase in the molar ratio of hydrogen-to-hydrocarbon causing an increase in the relative hydrocarbon concentrations on the acid and metal sites, and lastly
- a higher feed reactant carbon number meaning the number of elementary acid-catalysed steps available increase faster with carbon number than the HD/DHD reactions.

A non-ideal catalyst exhibits a slanted distribution unlike the bell-shaped product distribution of an ideal catalyst. This favours the production of low carbon number products due to extensive secondary cracking. This distribution, similar to that of the catalytic cracking product distribution, may be used to identify non-ideal catalysts (see section 2.6.3).

2.4 Selection of Palladium Metal Function

It is well known that the noble metals platinum and palladium are suitable for providing the HD/DHD function in a bifunctional hydrocracking catalyst. However it is limited to the use of clean feedstock as shown by Brosius and Fletcher (2013) - the results of which were used as a starting point for this research.

From figure 2.6 it can be seen that the maximum activity was found to be at 0.1 wt% palladium supported on H-MFI under standard LTFT conditions (i.e. T = 225°C, P = 20 bar, WHSV = 1 h^{-1}, H_2/C_{16}= 10 and H_2/CO = 2 when feeding CO). This activity was however accompanied by overcracking. The secondary cracking of palladium at this low loading was attributed to a poor metal:acid balance. Ideal hydrocracking was found to be in the region of 0.3-0.9 wt% with the decrease in activity trend for greater loadings attributed to the possibility of internal mass transfer limitations or palladium ion exchange during catalyst preparation.

The subsequent co-feeding of carbon monoxide was shown to increase the activity of higher loaded catalysts with a plateau being reached at 0.3 wt% palladium. The almost ideal product spectrum of the palladium catalyst changed dramatically upon the addition of carbon monoxide with secondary cracking becoming the dominating feature of the catalysts. It was concluded that the addition of carbon monoxide caused the migration of the Pd towards the external surface thus minimizing the mass transfer limitations. This conclusion was supported by the fact that after the addition of CO the catalysts containing a higher wt% palladium exhibited a similar product spectrum to catalysts with significantly less Pd using clean feedstock. Comparatively the platinum metal was seen to be completely poisoned by CO resulting in almost total deactivation of the catalyst. The palladium catalyst however does retain some of its activity even in the presence of CO, and thus, with reference to the project hypothesis, was used as the basis for this project.

The focus of this project is thus twofold i.e. to determine if it is possible to limit the migration of the palladium during the co-feeding of carbon monoxide and to ascertain if it is possible to weaken the CO-Pd bond strength thus preserving both the intrinsic activity and selectivity of palladium hydrocracking catalysts.

2.5 Iron addition to Supported Palladium Catalysts

2.5.1 Rate of Dehydrogenation/Hydrogenation

In an attempt to derive CO hydrogenation and olefin hydroformulation catalysts, Fukuoka et al. (1990) showed that at at temperatures of ca. 150°C and pressure of 1 bar, silica supported Pd_6Fe_6 is highly active for the hydrogenation of ethylene and propylene with the rate of hydrogenation being 10 to 100 times faster than that of the other bimetallic catalysts tested. During the CO hydrogenation reactions, the same catalysts showed a negligible CO conversion of 0.5% at 250 °C and 4.9 bar. This catalyst was thus described by the authors as a non-selective catalyst. These results, however negative in the study, are promising for hydrocracking reactions due to the need for a metal HD/DHD function. Fukuoka et al. (1990) provided further insight into the suitability of the Pd_6Fe_6 cluster for hydrocracking in showing that from the results of Mössbauer and EXAFS studies, Fe ions are highly dispersed and are located at the Pd-SiO_2 interface. Consequently, the Fe can be seen as a chemical anchor between the support and Pd which would minimize Pd migration.

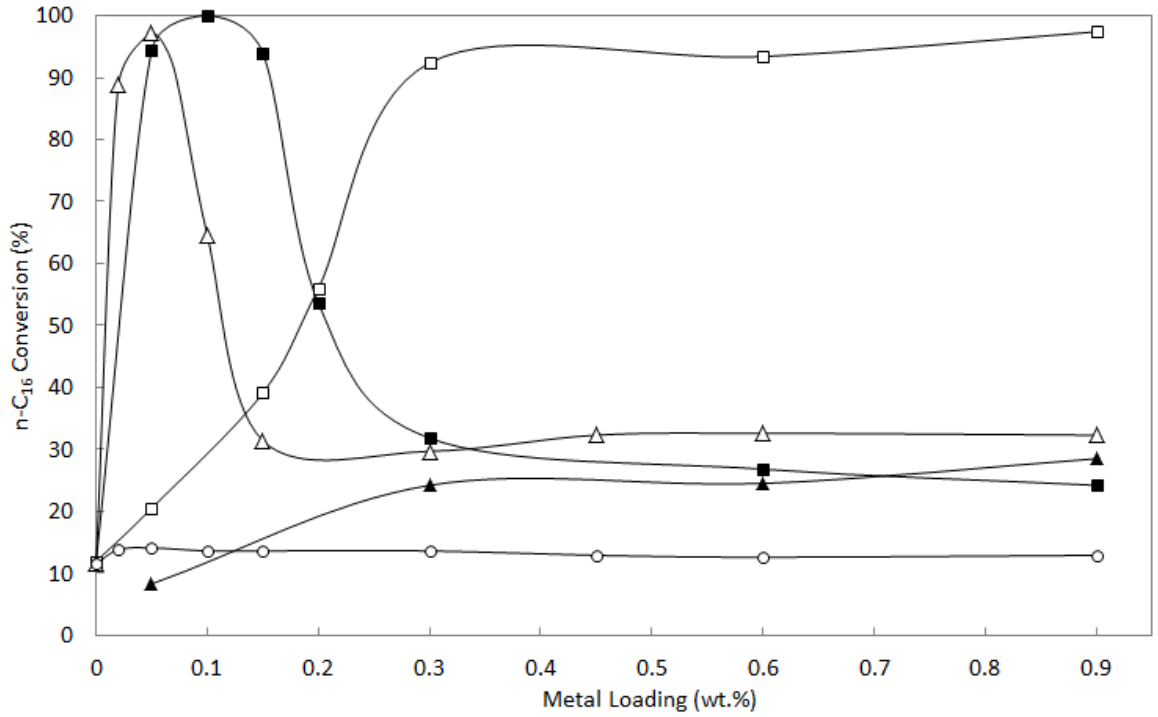

Key: (■) Pd/H-MFI; (□) Pd/H-MFI with CO after 1 day; (▲) Pd/H-MFI with CO after 8 days; (△) Pt/H-MFI;(○) Pt/H-MFI with CO.

Figure 2.6: Correlation between activity in n-hexadecane hydrocracking and metal loading redrawn from Brosius and Fletcher (2013).

2.5.2 Chemical Anchoring of Palladium

The chemical anchoring of palladium by iron has since been intensively studied by Wen et al. (2002). The authors found that the addition of Fe to Pd/ZSM-5 catalysts increased the nucleation rate but decreased the growth rate of Pd clusters in the catalysts. This led to highly dispersed Pd ions which did not migrate as expected under the given conditions. These results were attributed to the strong chemical interaction of Pd and Fe through d-orbital overlap. The group also found that the usually highly mobile $[Pd(NH_3)]^{2+}$ ion was not present, further supporting the claim that the use of iron as a chemical anchor for palladium is possible in supported catalysts. Fukuoka et al. (1990) confirmed that during H_2-reduction of Pd-Fe catalysts derived from $PdCl_2$ + $FeCl_3$ that no Fe-O bond was present with the Fe atoms being uniformly distributed forming a Pd-Fe alloy.

2.5.3 Pd-Fe Alloy Formation

Alloy formation can be viewed as the possible reason for the high hydrogenation rate of ethylene seen by Fukuoka et al. (1990). The formation of a Pd-Fe alloy has been shown to be present in zeolite Y (Xu et al., 1993) with the reducibility of Fe being improved significantly with Pd. This was attributed to be a characteristic of the Pd-Fe alloy (Garten, 1976). The evidence of an alloy also includes the decrease in the formation of Pd hydrides in the presence of H_2 . This is a well-known characteristic of palladium alloys and has been confirmed through Temperature Programmed Reduction (TPR) and Temperature Programmed Desorption (TPD) experiments. The strong interaction of Pd^0 and Fe^0 has also been confirmed through Mössbauer and FTIR data (Xu et al., 1993).

2.6 Zeolites

A zeolites is solid acid and can be defined as a natural or synthetic micro-porous aluminium and silicon metal oxide with a high degree of crystallinity (Scherzer and Gruia, 1996; Weitkamp, 2000). They consist of the metal aluminium or silicon cations, frequently referred to as T atoms, surrounded by four oxygen atoms. These tetrahedral structures are arranged in a regular pattern and form the basis for the zeolite. The stacking of the tetrahedra creates microscopic channels and pores of a standard size that allow selective molecules to pass through them. This has led to zeolites often being referred to as molecular sieves.

The silicon atom in the zeolite has a 4^+ oxidation state whereas the aluminium T-atom exists in the 3^+ oxidation state. The silicon tetrahedron is consequently electron neutral while the aluminium tetrahedron is anionic and thus the zeolite structure overall is electron deficient and needs a cation to maintain neutrality. These cations are easily exchanged and therefore give the zeolite a wide range of properties and uses.

The industrial applications of zeolites are constantly growing as the list of zeolite frameworks increase. Examples of the applications of zeolites include petrochemical hydrocarbon cracking, water purification, solvent removal and separation processes as well as various agricultural applications. Hagen (1999) classified zeolites into three useful subsets based on the aluminium-silicon ratio. This classification outlines the industrial importance of zeolites and shows the technological advances made in the synthesis of new zeolites. A brief summary of this can be found in Table 2.5.

Table 2.5: General summary of various zeolite structure types and their industrial uses Hagen (1999)

Name	Example Types	Si/Al ratio	Industrial Uses
Low-Silica	Zeolite A and X	$\approx$ 1-1.5	Drying, Purification
Intermediate Silica	Zeolite Y and L	2-5	Catalytic Cracking
High Silica	ZSM-5, dealuminated	$\geq$ 10	Organic Adsorbtion

Hagen (1999) indicated that the faujasite zeolites are mainly used in catalytic cracking and in hydrocracking with hydrogen with the products being gasoline, heating oil and kerosene. This agrees with Weitkamp and Puppe (1999) and Bekkum et al. (1991) who indicate that Y-zeolite is the most commonly used catalyst support in the processing of heavy hydrocarbons. The use of the Y-zeolite in the cracking of long-chained hydrocarbons is due to the relatively high stability of the lattice structure, the concentration of acid sites available and the bulky, highly branched nature of the crude oil based feed.

2.6.1 Effect of Zeolite Selection on Hydrocracking Selectivity

This project follows the work of Kukard (2008) who researched the effect of various medium and large pore size zeolites on long chain n-paraffin hydrocracking with the aim to impose shape selectivity into the bifunctional mechanism. Owing to the linear nature of the FT reaction products it was found that the medium pore size H-MFI zeolite exhibited and improved selectivity towards linear hydrocracking products (i.e. high cetane number) while large pores (H-USY and H-MOR) as well as intersecting medium and large pores (H-BEA) showed similar selectivities towards mono-methyl branched species.

It was also noted that the activity of the zeolites with medium pore sizes (H-MFI and H-BEA) was significantly higher than those containing only large pores (H-USY and H-MOR). This was attributed to the orderly and efficient configuration of the absorbed molecules resulting in increased access to

active acid cites. The use of H-MFI thus presents a promising opportunity for the production of high quality diesel from FT wax.

2.6.1.1 H-MFI Zeolite

The H-MFI (or ZSM-5) structure is defined by its three-dimensional orthorhombic pore topology. The pores are as a result of the intersection of straight and sinusoidal channels created by elliptical 10-member ring structures which form pore openings of 5.1 $\times$ 5.5 Å and 5.3 $\times$ 5.6 Å respectively. The structure has a Si/Al ratio of 78 (Auerbach et al., 2003; Szostak, 1992). A representation of the H-MFI zeolite unit cells and polyhedral pore structure can be seen in figures 2.7 and 2.8 respectively.

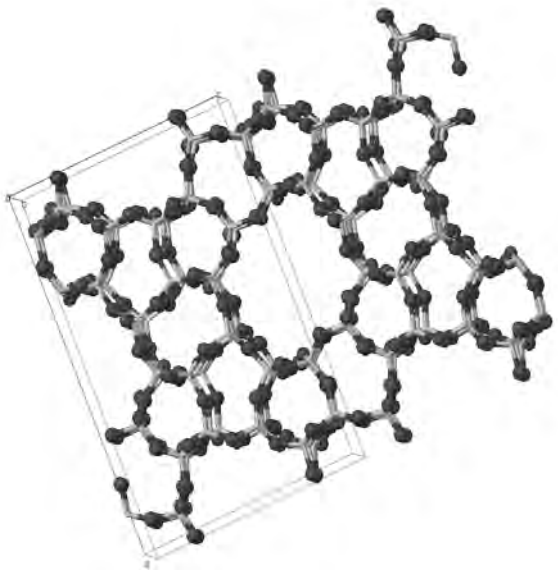

Figure 2.7: Ball and stick representation of the H-MFI zeolite structure showing the pore channel between unit cells (Baerlocher and McCusker, 2013).

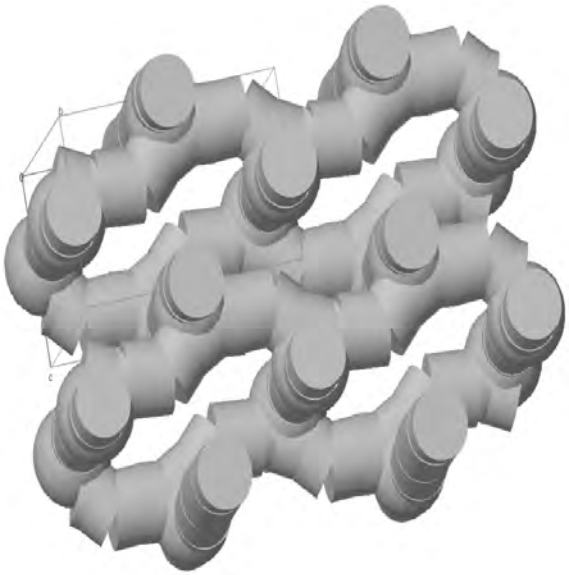

Figure 2.8: Representation of the intersection of sinusoidal and straight pore channels in H-MFI zeolite (Baerlocher and McCusker, 2013).

2.6.2 Hydroisomerization

In order to improve the cold flow properties of middle distillate fuel, dewaxing through shape selective hydrocracking is possible. This process is needed due to the tendency of the LTFT process to produce long chain n-paraffins which coagulate at low temperatures i.e. the wax has a high pour point. In order to reduce this pour point, linear n-paraffins need to be isomerized into branched molecules at the expense of the cetane number (as noted in section 2.2.3). The skeletal isomerization step of hydrocracking using a bifunctional catalyst is an economical and convenient dewaxing process. A minimization of the hydrocracking reaction may be needed when high yields of skeletal isomers are to be achieved. The hydroisomerization of linear molecules can easily be done using the appropriate zeolite due to their shape selectivity (Bouchy et al., 2009).

Csicsery (1984) noted that that there are three main shape selectivity effects which are governed by the sterical hindrance of molecules inside the confined zeolite spaces. These effects are the reactant, product and transition-state shape-selectivity. Shape selective processes may contain one or a combination of these effects depending on whether the reactants or products are subject to diffusion limitations or whether the reaction itself is sterically hindered.

For the production of high quality diesel, the H-MFI zeolite (see section 2.6.1.1) may be appropriately used when hydrocracking long chained molecules (i.e. carbon number ≥ 10) as it causes bulky reaction intermediates to be trapped inside the pore structure resulting in many successive isomerizaton steps before cracking. This subsequently causes the preference towards linear molecule products.

2.6.3 Interdependence of Selectivity and Conversion

The successive hydrocracking and hydroisomerizaton steps of the bifunctional mechanism results in an interdependence of the two functions based on the reaction conditions and catalyst type. In the ideal case (see section 2.3.2), where the metal function is not the rate limiting step and in the presence of pure primary hydrocracking, the product distribution is fully symmetrical around half of the original molecule (Bouchy et al., 2009; Weitkamp, 2012).

Figure 2.9 shows the actual product distribution of ideal hydrocracking of n-C_{16} over a Pt/CaY catalyst in which no $C_{1\text{-}2}$ and $C_{14\text{-}15}$ is formed. C_3 and C_{13} are formed in small amounts while the $C_{4\text{-}12}$ fragments show a flat product spectrum. This to be expected due to the rates of reaction for the classification of β-scission reactions (see figure 2.5). This is a common salient feature of ideal hydrocracking in which the molar ratio of cracked products to that of n-C_{16} is equal to two i.e. β-scission occurs once per n-C_{16} molecule. This form of hydrocracking may only occur if the intermediate olefin is in abundance i.e. at low cracking conversions and high isomerization.

Comparatively, at high cracking conversions the metal function becomes the rate limiting step as the supply of olefins for cracking is minimized. This results in lower isomerization (see figure 2.10) and secondary cracking. The product distribution for the non-ideal hydrocracking of n-C_{16} over a Co-Mo-S/SiO_2-Al_2O_3 catalyst can also be seen in figure 2.9. This product distribution is entirely different from that of an ideal catalyst as the the majority of the product is skewered towards the $C_{3\text{-}6}$ fraction as a result of significant secondary cracking. This product distribution is typical of a non-ideal catalyst.

From this it can be seen that at high cracking conversions using an ideal hydrocracking catalyst, the product distribution will resemble that of a non-ideal hydrocracking catalyst (or an acidic catalytic cracking catalyst). Thus in order to maintain ideality it is desirable to maintain high levels of isomerization to ensure adequate olefin supply for the primary β-scission step.

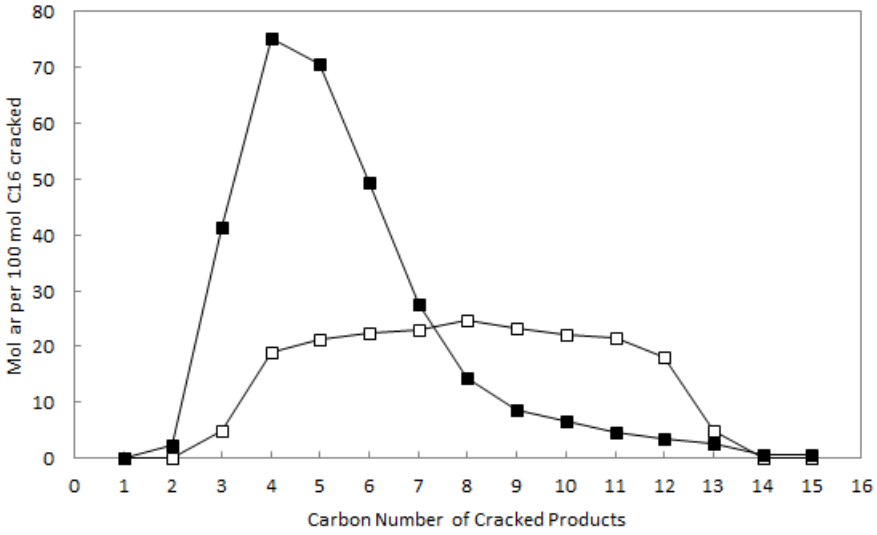

Key:(□) Pt/CaY Ideal hydrocracking catalyst (T = 230 °C; mol cracked products/mol cracked C_{16} = 2.0; (■) Co-Mo-S/SiO_2-Al_2O_3 Non-ideal hydrocracking catalyst (T = 400 °C; mol cracked products/mol cracked C_{16} = 3.0). Cracking conversion circa 50%.

Figure 2.9: Molar carbon number product distribution for the hydrocracking of of n-C_{16} adapted from (Bouchy et al., 2009; Weitkamp, 2012).

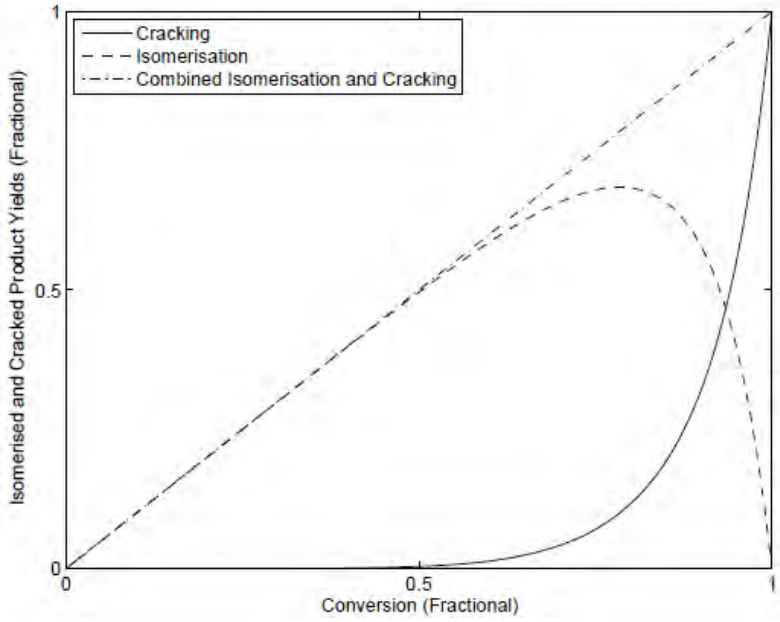

Figure 2.10: Representation of Conversion vs Yield for cracking of long chained n-paraffins over a bifunctional catalyst, adapted from Martens and Jacobs (2001).

Chapter 3
Research Objectives

"When you've eliminated the impossible, whatever remains, however improbable, is the truth."
Sherlock Holmes - Elementary

3.1 Hypothesis

From the available literature and data obtained from previous experiments, it is clear that there exists an opportunity to synthesis CO tolerant palladium-iron catalysts for Fischer-Tropsch wax hydrocracking.

As it is known that Fe acts as a chemical anchor in supported palladium catalyst the following hypothesis was theorized:

1. **The addition of Fe to Pd/Zeolite catalysts will prevent the migration of Pd (upon the co-feeding of CO) to the external surface and act as a chemical anchor through strong d-orbital interactions.**

The second hypothesis of this project is based on the strong interaction between Pd and Fe and the formation of the PdFe alloy. It is thus hypothesized that:

2. **The addition of Fe to Pd/Zeolite catalysts will weaken the Pd-CO chemical bond by changing the metal electron density thus reducing poisoning of the catalysts.**

Finally, the promotional effect of the addition of H_2O will be tested based on the hypothesis that

3. **The co-feeding of water will counteract any residual Pd migration due to the ability of water to hydrate the protons present thus deactivating the catalyst by diminishing acid strength and thereby restore the metal-acid balance.**

A number of key questions will need to be answered in order to prove or disprove these hypotheses.

3.2 Key Questions

The focus of this project will be to answer the following questions:

- What effect does the of co-feeding carbon monoxide have on monometallic palladium loaded zeolites in the hydrocracking of n-hexadecane in terms of conversion, activity and selectivity?
- What effect does the of co-feeding carbon monoxide have on bimetallic palladium and iron loaded zeolites in the hydrocracking of n-hexadecane in terms of conversion, activity and selectivity?

- In the tested bimetallic catalysts, what effect does varying the palladium and iron loading have on the hydrocracking hydrocracking of n-hexadecane in terms of conversion, activity and selectivity?
- Does the addition of iron promote the carbon monoxide tolerance of the palladium hydrocracking catalyst?
- What effect does of co-feeding water have on monometallic palladium loaded zeolites in the hydrocracking of n-hexadecane in terms of conversion, activity and selectivity?
- What effect does of co-feeding water have on bimetallic palladium and iron loaded zeolites in the hydrocracking of n-hexadecane in terms of conversion, activity and selectivity?
- Does the co-feeding of water improve the carbon monoxide tolerance of the monometallic and bimetallic hydrocracking catalyst?

3.3 Scope and Limitations

This project will be limited to the effect of the possible CO (primary) and H_2O (secondary) impurities in the wax hydrocracking process feed of the Fischer-Tropsch synthesis. The effect of all other possible impurities on the hydrocracking catalysts will not be considered as part of this research. This study will also focus only on the palladium noble metal and its interaction with iron on the H-MFI-90 zeolite and its subsequent effect on the conversion, activity and selectivity in the hydrocracking process.

Chapter 4
Experimental

"I recognize that tone of voice, Niklaus. Clearly you have some diabolical machination. What is it?"
Elijah Mikaelson - The Originals

4.1 Catalysts

4.1.1 Palladium-Iron Naming Convention

The catalyst tested were uniquely labelled according to the ratio of support acid sites per gram to the palladium metal sites per gram (Al/Pd) as well as the ratio of support acid sites per gram to the iron metal sites per gram (Al/Fe). The general label form can be seen below:

$$\text{PdFe/H-MFI (*Al/Pd ratio*,*Al/Fe ratio*)} \tag{4.1}$$

Using the above formula an example of a prepared catalyst is PdFe/H-MFI (4,24).

4.1.2 Various Catalysts Tested

Previous experiments found that the optimum activity of Pd/H-MFI catalyst occurs at 0.96 wt% palladium (Brosius and Fletcher, 2013). From literature it is known that Pd forms stable Pd_6 clusters at temperatures below 643 K (Okumura et al., 2004) and thus a Pd/Fe molar ratio of six is needed to ensure that each palladium cluster contains one Fe ion. From this the correct amount of $Pd(NH_3)_4(NO_3)_2$ to be used in incipient wetness impregnation (IWI) can be calculated. The ratio of Fe to Pd_6 was adjusted to obtain the various catalysts to be tested (see table 4.1).

Table 4.1: Specifications for the preparation of the various hydrocracking catalysts tested.

Catalyst name	**Al/Pd**	**Al/Fe**	**Pd wt%**	**Pd added [g]**	**Pd solution added [g]**	**Fe/Pd_6 clusters**
PdFe/H-MFI (4,24)	4	24	0.96	0.0211	0.3295	1
PdFe/H-MFI (8,24)	8	24	0.48	0.0106	0.1647	2
PdFe/H-MFI (16,24)	16	24	0.16	0.0035	0.0549	4
PdFe/H-MFI	4	∞	0.96	0.0211	0.03295	[-]
PdFe/H-MFI (4,12)	4	12	0.96	0.0211	0.03295	2
PdFe/H-MFI (8,12)	8	12	0.48	0.0106	0.01647	4
PdFe/H-MFI (16,12)	16	12	0.16	0.0035	0.00549	8

4.1.3 Catalyst Preparation

Solid-state ion-exchange was used to add iron to the zeolite which was subsequently impregnated with the palladium. The solid state ion-exchange method used is similar to that of Kögel et al. (1999) who reported activities for aerobic preparation comparable to those of anaerobic preparation.

To prepare the example given in section 4.1.1 (i.e. the PdFe/H-MFI (4,24)) the following method was used. 10 grams of H-MFI was physically mixed (using a mortar and pestle) with 0.0300 grams of $FeCl_2{\cdot}4H_2O$ before being milled in a McCrone micronizing mill for 1 hour. The mixture was then heated in an oven (Labofurn) to 550 °C in 3 hours and left for 6 hours at this temperature before being allowed to cool to 60 °C. The product was then removed from the oven and allowed to cool to ambient. This sample was then washed thoroughly using 1.5 litres of deionized water and a vacuum pump before being dried overnight at 120 °C.

A 2.2 gram sample of the Fe/H-MFI was then impregnated with palladium by mixing with 0.3295 grams of liquid $Pd(NH_3)_4(NO_3)_2$. Deionized water was then added to bring the total liquid volume to 1.54 grams. This was thoroughly mixed to ensure incipient wetness and left to dry overnight. The resulting sample was then pelletized using a Specac Manual Press (load of 15 tons) and sieved to obtain 1 gram of PdFe/H-MFI (4,24) in the 850-500 μm size range.

4.2 Catalyst Testing

4.2.1 Hydrocracking Test Apparatus

All experiments were conducted in a dedicated plug-flow fixed trickle-bed reactor equipped with a homogeneously operating evaporator and on-line gas chromatography flame ionizing detector (GC-FID) analysis. A process flow diagram of the feed system as well as the reactors can be seen in figure 4.1. A schematic representation of the GC-FID sampling system can be seen in figure 4.2. The gas feed components (Air/O_2, N_2, H_2 and CO) were supplied through a mass flow controller connected directly to the overhead gas manifold. The liquid components (n-hexadecane and H_2O) were fed by high pressure liquid chromatography pumps (Lab Alliance Series 1 HPLC pumps). The liquid feed pots were placed on balances in order to verify the liquid feed rate.

The reactor itself is a stainless steel cylindrical tube with an approximate internal diameter of 16.8 mm and a length of 360 mm. An internally embedded thermowell with an outer diameter of approximately 3 mm runs through the length of the reactor. The reactor temperature was controlled by the use of 4 individual heating blocks connected to Gefran temperature controllers. Blocks 1-3 in figure 4.1 uses Gefran 800P while block 4 a uses Gefran 600 temperature controller (see appendix A for temperature profile and calibration method).

The reactor product is vaporized by N_2 dilution to ensure no liquid products are present before the sampling and on-line analysis. The vaporizer, sample line as well as the wax traps as seen in figure 4.1 are all individually controlled by Gefran 600 temperature controllers.The N_2 dilution is achieved through the use of pressure regulators and capillary tubes which were calibrated to supply N_2 at a rate of 200 ml/min to the vaporizer (see appendix B for calibration method).

4.2.1.1 Test Unit Auxiliary Components

Pressure Relief Valves

A number of pressure relief valves are situated on the rig which provides a safety mechanism in the event of excess pressure build-up. Once a certain maximum pressure is reached on the rig, the pressure relief valve releases gas to the vent in order to prevent over-pressurization. This is achieved by the use of a spring loaded cap. The spring pushes against a membrane with a set force which is counterbalanced by the pressure of the gas in the line. Once the force exerted on the membrane by the line pressure exceeds that of the spring the gas is released and vented.

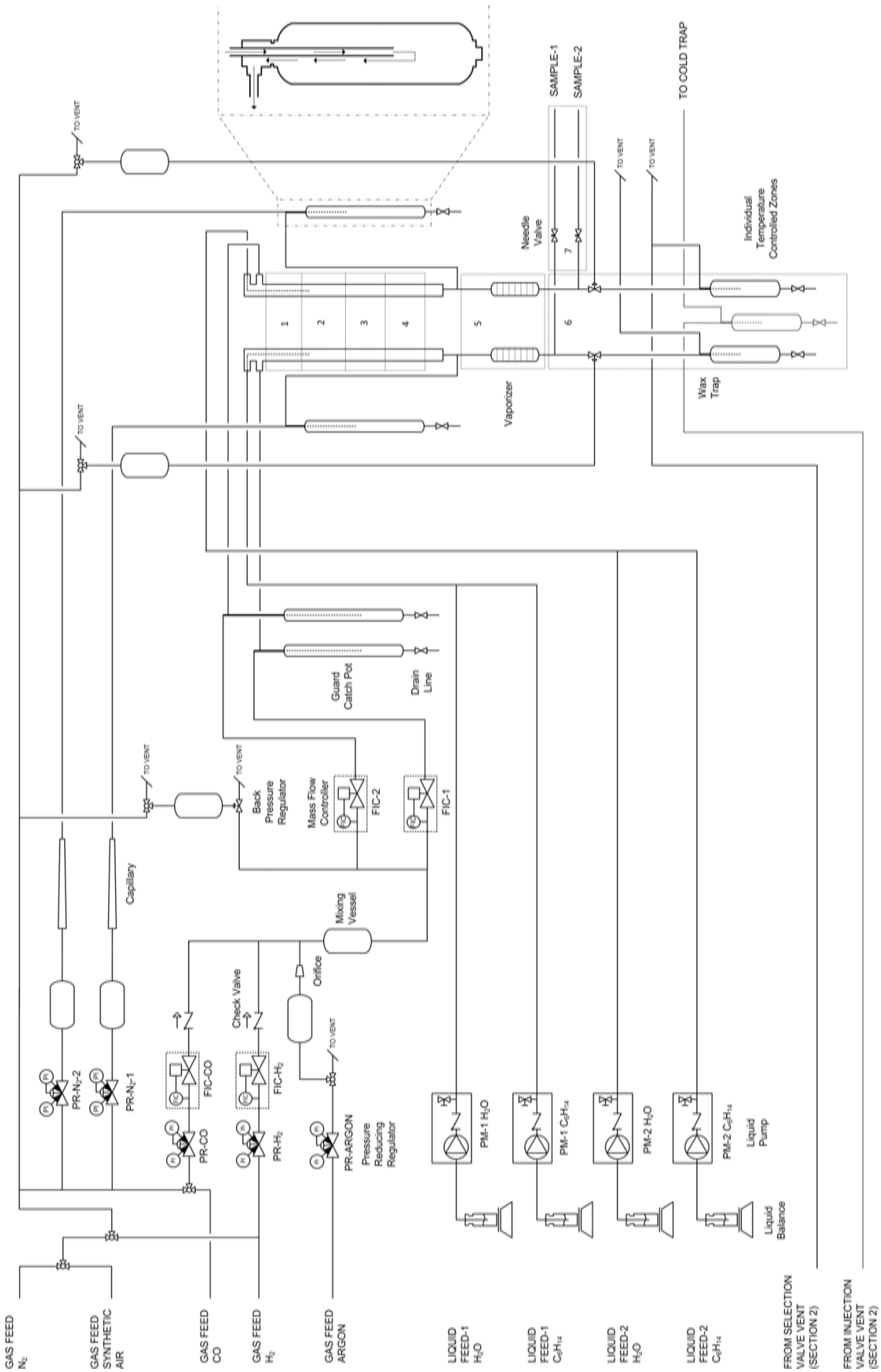

Figure 4.1: Process flow diagram of hydrocracking test unit.

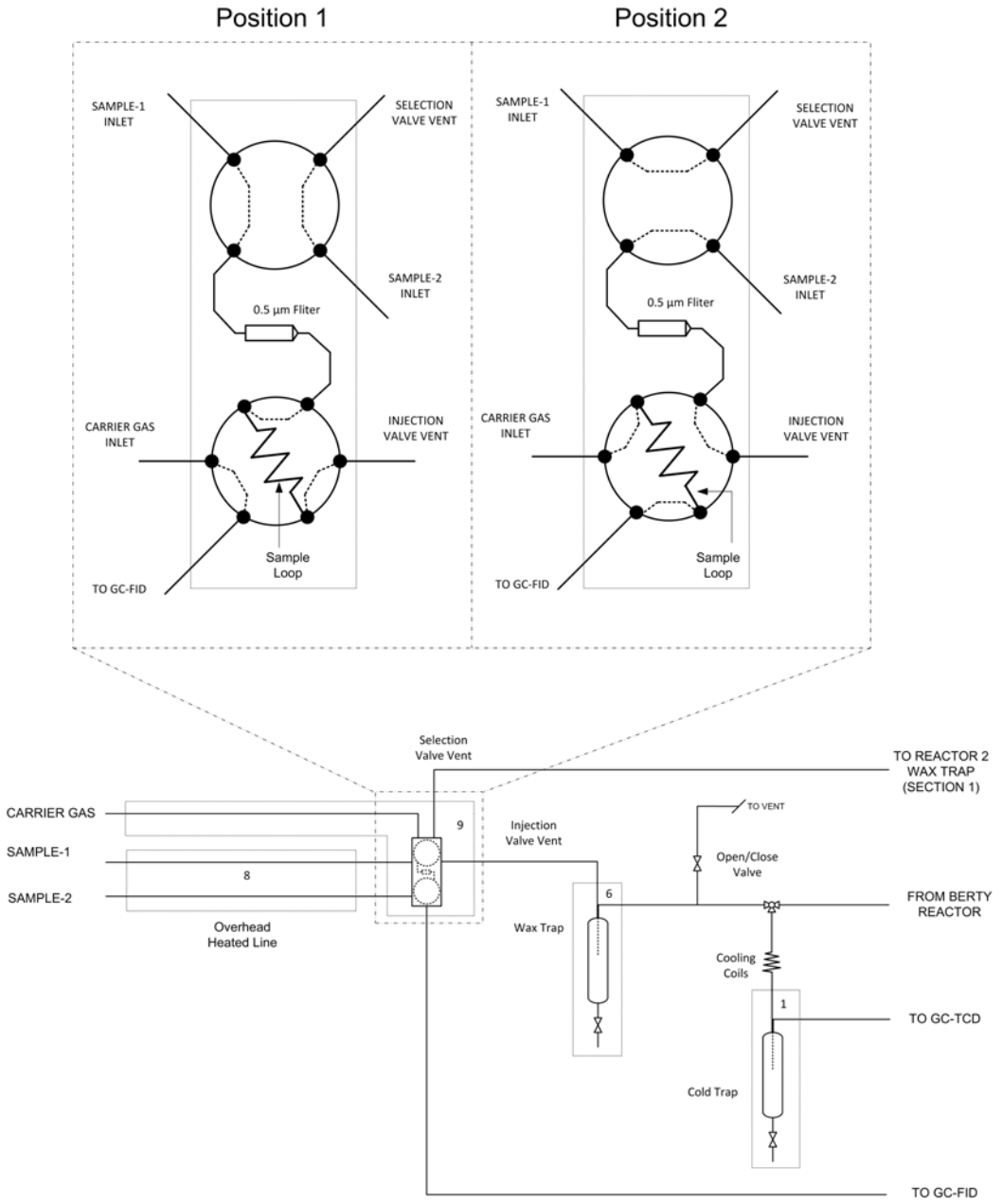

Figure 4.2: Schematic of on-line hydrocracking sampling system.

Guard Pots
Under normal conditions the gas feed from the mass flow controllers enters the top of the T piece and flows through a dip-tube into the guard vessel. The flow subsequently proceeds under pressure towards the T-piece outlet. This provides a safety mechanism for the mass flow controllers as it ensures that any liquid reverse flow from the reactors would first flow through the T-piece outlet and collect in the vessel before flowing up the dip-tube. This minimizes the possibility of damage to the mass flow controllers (see figure 4.4). Similar guard pots (on the dilution gas line) are placed between the capillaries and the reactor effluent (see figure 4.1).

Back Pressure Regulators
The back pressure regulators are used to maintain a constant pressure in the reactors. The pressure is set by the nitrogen flow in the rig. As this flow remains unchanged throughout the experiment the pressure on the top of the membrane remains constant. The gas flow through the bottom of the regulator depends on the pressure of the gas. If the pressure of the gas is less than that of the pressure exerted on the membrane by the N_2 gas, no flow through the regulator will occur. This will subsequently cause a build-up of pressure on the underside of the membrane until it reaches the desired N_2 set pressure. The pressure on both sides of the membrane will be equal which will then allow flow through the regulator.

Selection Valve
The selection valve is a 4-port 2-way valve (see figure 4.2) that chooses which reactor will be sampled. In position 1 the sample line from reactor 1 is selected and the flow proceeds through to the injection valve. The sample line from reactor 2 is sent to vent in this position. In position 2 to the reverse occurs i.e. reactor 2 is sampled and the flow from reactor 1 is vented. The selection valve is followed by a 0.5μm metal frit filter which prevents particulate matter from entering the injection valve and damaging the GC-FID column.

Injection Valve
The injection valve is a 6-port 2-way valve (see figure 4.2) that is used to take standard volume samples of the reactor effluent. In position 1 the reactor effluent flows through a sample loop before being vented. In this position only the carrier gas flows into the gas chromatogram. Once the injection valve is switched to position 2 (sample injection) the carrier gas flows through the sample loop into the gas chromatogram while the reactor effluent is vented. The volume of gas in the sample loop when the valve is switched from position 1 to position 2 is the volume of gas sampled.

Reactor Head
Owing to the fact that hexadecane and water are immiscible feed components in the liquid phase they need to be vaporized before entering the catalyst bed. The water vaporization is achieved by allowing the liquid water to flow through a dip-tube which is in contact with the silica bed in the reactor. The hexadecane is fed directly onto the silica bed and evaporated. This ensures that the mixing of the feed components all occur in the gas phase and thus homogeneous mixing is possible. The evaporation of both the hexadecane and the liquid water occur in the reactor body well before the catalyst bed.

4.2.2 Catalyst Pretreatment

The catalyst used was calcined and reduced in-situ. It was found that this pre-treatment step had a major impact on the overall performance of the catalyst and thus needed to be optimized. Philippaerts et al. (2010), who conducted sorption and hydrogenation experiments on MFI zeolites, states that slow calcination (0.3 °C/min heating ramp) and reduction rates (0.4 °C/min heating ramp) provide the best results for Pt/ZSM-5 catalysts in terms of hydrogenation activity and selectivity due to improved Pt distribution and Pt particle size. This heating ramp was applied to the standard

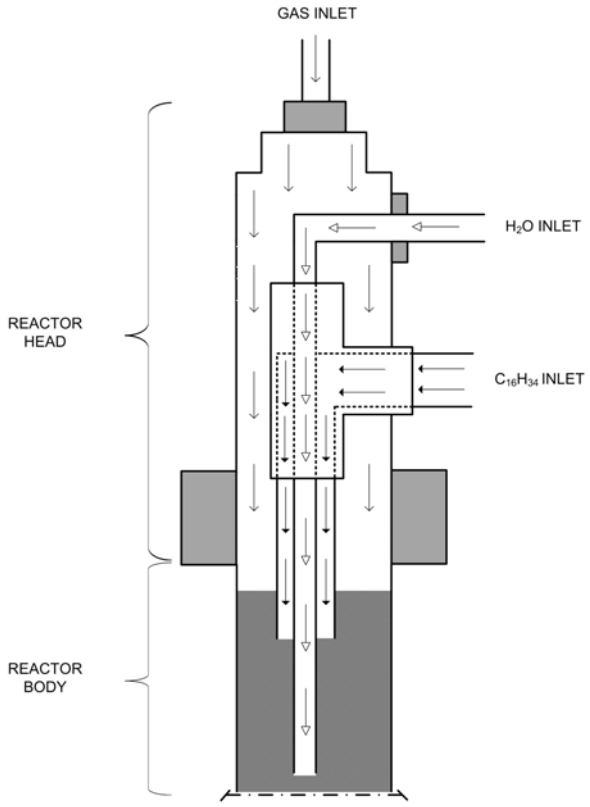

Figure 4.3: Schematic of reactor head showing the entrance pathways of the feed components allowing for homogeneous mixing in the gas phase.

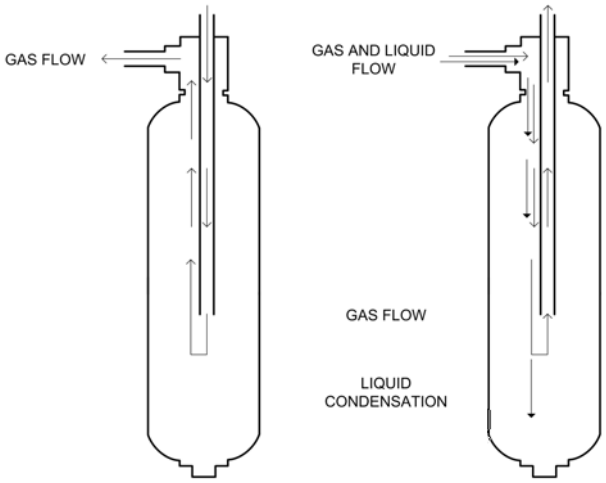

Figure 4.4: Schematic of Guard Pot under normal flow conditions (left) and abnormal (reverse flow) conditions (right) showing the liquid condensation in the pot.

Pd/H-MFI and was found to cause a remarkable improvement in terms of selectivity of the catalyst at higher conversions as compared to catalysts prepared using the original higher heating ramps (ramp of 1.83 and 0.5 °C/min for calcination and reduction respectively).

4.2.2.1 Reactor Loading

The catalyst was mixed with silicon carbide (SiC) in the ratio of 1:10. For all experiments conducted 1 gram of catalyst was used and thus mixed with 10 grams of SiC. The reactor was initially plugged with a small amount of glass wool in order to prevent blow-out into the vaporizer. This was then followed by 20 ml of SiC and then the catalyst-SiC mixture. The reactor was then filled with SiC before the reactor head was fitted using a gasket to eliminate leaking. The reactor head was then hand-tightened before being tightened using an appropriate wrench (approximately 60 °rotation). Loading the reactor in this manner ensured that the catalyst would be placed in the centre of the isothermal zone.

4.2.2.2 Calcination

The catalyst was calcined in-situ using a heating ramp of 0.3 °C/min from ambient to 350 °C and left at this temperature for 30 mins before being allowed to cool to 60 °C. This was done under pure oxygen flow of 100 ml/min to each reactor at a pressure of 1 bar.

4.2.2.3 Reduction

After calcination the reactor was flushed with nitrogen for 30 mins to remove any oxygen in the reactor. This is to ensure that there is no production of water during the reduction step. The reactors were subsequently pressured with nitrogen to 20 bar (i.e. set back pressure regulators for each reactor) before the introduction of hydrogen. The catalyst was then heated to 200 °C at 0.4 °C/min under a hydrogen flow rate of 100 ml/min. Sampling was then started once the final temperature was reached.

4.3 Test Procedure

4.3.1 Start-up Procedure

The following procedure was used for the start-up of all the experiments conducted. Note: this procedure outlines that of normal start-up in which the vaporizer, the GC-FID selection/injection valves and overhead lines are at their required temperature.

- Clean reactor and reactor head using acetone to remove residual SiC and reactants/products.
- Remove glass wool plug using compressed air.
- Follow reactor loading procedure found in section 4.2.2.1.
- Place the reactor into its appropriate heating block and fastened with a lock nut at the base (using a gasket) and at the inlet feed points (using a gasket at the liquid inlet feed points). The use of heat resistant gloves may be necessary for the base nuts.
- Cover the reactor base with the appropriate insulation (i.e. glass wool).
- Set the N_2/CO 3-way valve to N_2.
- Open the N_2 gas manifold valve.
- Set gas feed back pressure regulator is set to 10 bar (i.e. blend pot).

- Open the Air/O_2 gas manifold valve.
- Follow the procedure outlined in section 4.2.2.2 for the catalyst calcination.
- Close the Air/O_2 gas manifold valve.
- Set gas feed back pressure regulator (i.e. blend pot) to 30 bar.
- Follow the procedure outlined in section 4.2.2.3 for the catalyst reduction.
- Once the reduction is complete the temperature program is set to manual on the Gefran 800P temperature controllers and heating block 4 is set to its reaction temperature (see appendix A).
- The gas inlet feed mass flow controllers are then set. Under normal conditions, a total N_2 flow rate of 20 ml/min, a total H_2 flow rate of 40 ml/min and an individual left and right reactor flow rate of 24 ml/min is set.
- Prime the n-hexadecane HPLC pumps for approximately 30 seconds. Note: the inlet liquid feed valves are set away from the reactor and the feed liquid is collected in a bottle during priming.
- Set the the inlet n-hexadecane liquid feed valves towards the reactor and HPLC pumps to 0.02 ml/min.
- Record the time feed pot balance for n-hexadecane feed verification calculations.
- Finally, start the on-line gas chromatogram sampling.

4.3.2 On-line Procedure

The normal operating on-line procedure is limited to changing the temperature of the reaction as well as adding/removing H_2O and CO as the reaction space velocity and pressure is set (i.e. standard low temperature Fischer Tropsch conditions).

4.3.2.1 Temperature

- The temperature is adjusted by means of a set of Gefran temperature controllers. The temperature of the reactor heating blocks are adjusted such that the reaction temperature changes in intervals of 5 °C (see appendix A).
- Each new temperature is allowed to settle for approximately 12 hours to ensure re-stabilization, reaction equilibrium and adequate sampling.

4.3.2.2 Water Addition/Removal

- Prime the H_2O HPLC pumps for approximately 30 seconds. Note: the inlet liquid feed valves are set away from the reactor and the feed liquid is collected in a bottle during priming.
- Set the inlet H_2O liquid feed valves towards the reactor and the HPLC pumps to 0.01 ml/min.
- Record the time and feed pot balance for H_2O feed verification calculations.

4.3.2.3 CO Addition/Removal

- To add/remove CO, the incoming 3-way N_2/CO valve is set from N_2 to CO.

4.3.3 Shut-down Procedure

The following procedure outlines that of a normal shut-down i.e. excluding the cooling of the vaporizer, GC-FID selection/injection valves and the overhead lines.

- Ensure that the running on-line GC-FID program is stopped or has been completed.
- Switch all HPLC pumps off.
- Close all incoming liquid feed valves.
- Set all gas mass flow controllers to closed.
- Close all gas manifold valves.
- Slowly lower reactor pressure to atmosphere.
- Slowly lower blend pot pressure to atmosphere.
- Set all reactor temperatures to ambient and allow approximately 6 hours to cool.

4.4 Gas Analysis

4.4.1 Gas Chromatography

The reactor products were analysed using a Varian 3900 on-line gas chromatography flame ionizing detector (GC-FID) and the Galaxie Chromatography Data System software package. See section 4.5 for product analysis calculations.

4.4.2 Sampling Procedure

The sampling procedure makes use of a 4-way selection valve and a 6-way injection valve as seen in figure 4.2. The reactors were sampled alternatively using an automated system. In order to sample the individual reactors the following method was inserted loaded into the Galaxie Chromatography Data System software package: (Note: approximately 30 seconds separate each successive step - excluding product analysis.)

- The selection and injection valves are set to sample 1 inlet and vent respectively. This allows the sample loop to be filled with the product from reactor 1.
- The injection valve sample loop is switched the GC-FID (i.e. sample 1 injection). Reactor 1 is vented through the injection valve while reactor 2 remains vented through the selection valve.
- The selection valve is then switched to sample 2 inlet.
- The injection valve sample loop is switched back to vent allowing the sample loop to be filled with the product from reactor 2. The carrier gas and the product sample flow through the GC-FID.
- The product from reactor 1 is analysed and the system is flushed before the injection valve sample loop is switched the GC-FID (i.e. sample 2 injection). Reactor 2 is vented through the injection valve while reactor 1 remains vented through the selection valve.
- After the reactor 2 product analysis and system flush, the selection valve is then switched back to sample 1 inlet.
- The injection valve sample loop is then switched back its initial state allowing the sample loop to be filled with the product from reactor 1. Both the selection valve and injection valve are in their initial state at this point at which the process repeats itself.

4.4.3 Analysis Conditions

The gas analysis control method was set using the column oven program found in table 4.2. The initial column temperature is set to 40 °C with a stabilization time of 30 seconds before each sample run. Each sample run had a total sampling time of 47.21 mins.

Table 4.2: Gas chromatography column oven program conditions for reactor product analysis.

Heating Rate (°C/min)	Step (°C)	Time (min)	Total Time Elapsed (min)
Initial	40	2.00	2.00
8.0	175	0.00	18.88
3.0	260	0.00	47.21

4.5 Data Work-up

The raw data output from the GC-FID consisted of a standard gas chromatogram with peak identification and variable baseline for integration. The area of each chromatogram peak is directly proportional to the number of individual carbon atoms in the molecule and thus the overall mass conversion of the feed n-hexadecane was determined using equation 4.2.

$$X_{C_{16}} = \left(1 - \frac{Area\, n\text{-}C_{16}\, peak}{\sum_{i=1}^{n} Area\, C_i\, peak}\right) \tag{4.2}$$

For each run, individual products up until a carbon number of 7 were identified. Products consisting of carbon numbers of 8-12 were grouped by isomerization i.e. straight chain paraffin, straight chain olefin, mono-branched paraffin isomers, multi-branched paraffin isomers and olefinic isomers. Products consisting of carbon numbers of 13-16 were grouped to a lesser more general extent i.e. straight chain, mono-branched and multi-branched. The grouping of products was necessary due to the difficulty in separating and identifying individual molecule fractions with high carbon numbers. The selectivity towards certain products and product groups were determined using equation 4.3. For the purposes of presentation, the final product selectivity for each run was further grouped into linear and branched molecules for each carbon number.

$$S_{C_i} = \frac{Area\, n\text{-}C_i\, peak}{\sum_{i=1}^{n} Area\, C_i\, peak - Area\, n\text{-}C_{16}\, peak} \tag{4.3}$$

To determine the yield of each product or product group for literature comparison of conversion vs yield graphs, equation 4.4 was used.

$$Y_{C_i} = S_{C_i} \times X_{C_{16}} = \frac{Area\, n\text{-}C_i\, peak}{\sum_{i=1}^{n} Area\, C_i\, peak - Area\, n\text{-}C_{16}\, peak} \times \left(1 - \frac{Area\, n\text{-}C_{16}\, peak}{\sum_{i=1}^{n} Area\, C_i\, peak}\right) \tag{4.4}$$

Chapter 5
Experimental Results and Analyses

"I don't need sleep, I need answers. I need to determine where in this swamp of unbalanced formulas squatteth the toad of truth."
Dr Sheldon Cooper - The Big Bang Theory

5.1 Base Case Results of Monometallic Pd/H-MFI

A desired ideal hydrocracking catalyst, as defined in section 2.3.2, can be made in the form of a monometallic palladium on support H-MFI. From figure 2.6 the catalyst selected as the base case is 0.96 wt% palladium on H-MFI as this catalyst behaves ideally at the low temperature Fischer-Tropsch conditions (20 bar, WHSV = 1 h^{-1}). The overall conversion at different temperatures for the base case catalyst can be seen in figure 5.1. This graph shows the increase in conversion as a function of temperature and sample run number. The importance of this increase in conversion is how it affects the cracking product selectivity and thus ideality (further discussed in section 5.1.1).

As a general rule it can be seen that at a lower temperature the catalyst is more ideal, evident by the extent of secondary cracking (see section 2.3.2 for explanation). At a temperature of 215 °C the base case has a cracking product selectivity seen in figure 5.2. This mass product distribution can be seen as the ideal product distribution for an H-MFI catalyst. It must be noted however that secondary cracking is present at this condition but the extent of this secondary cracking can be seen as minimal owing to the fact that the metal function is not rate limiting and thus the catalyst product distribution may still be considered ideal.

At higher conversions the extent of secondary cracking is significantly greater as shown by the increase in selectivity towards lighter products. At a temperature of 240 °C, the cracking product selectivity is severely skewed towards the lower carbon fractions (see figure 5.3). At this point the metal function is the rate limiting step and the catalyst is no longer ideal.

5.1.1 Defining Reference Ideality for Catalyst Comparison

The boundary between ideality and non-ideality can be defined as the point at which the criteria set out section 2.3.2 are no longer valid. From a practical perspective this boundary can be seen as the point at which the metal de-/hydrogenation function of the bimetallic mechanism becomes the rate limiting step, after which a noticeable increase in secondary cracking will occur due to the lack of olefinic compounds. In order to determine this point the concept of the C_4/C_{12} ratio was arbitrarily defined to be the ratio between the mass fractions of the 'light' C_4 and 'heavy' C_{12} compounds. This is a standard practice within the hydrocracking group. The conversion point at which this ratio drastically increases due to significant secondary cracking (i.e. increase in light carbon fractions) was defined as the boundary between ideality and non-ideality. From figure 5.4 it can be seen that this point exists at approximately 30% conversion (i.e. 225 °C) for the base case 0.96 wt% Pd/H-MFI catalyst. This corresponds to a C_4/C_{12} ratio of approximately 1. For catalyst comparison this ratio was used as a guideline to determine the extent of secondary cracking and thus the ideality of the catalyst i.e. a catalyst with a C_4/C_{12} ratio of 1 is considered ideal.

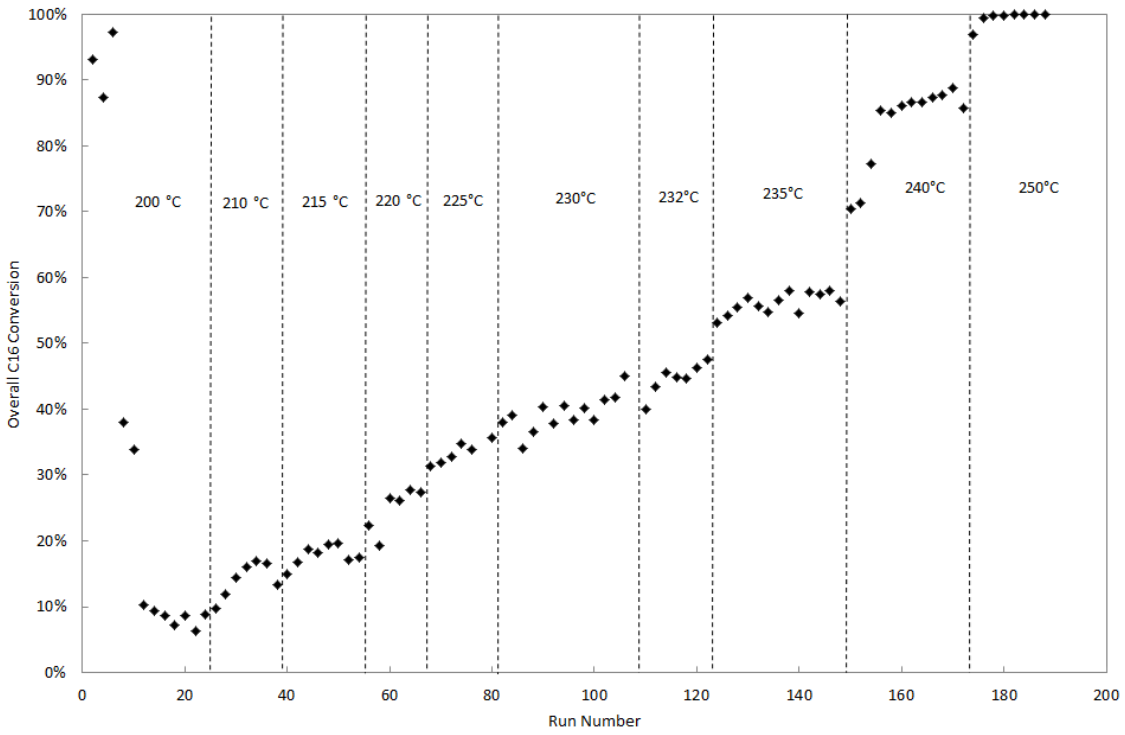

Figure 5.1: Graph of the overall conversion of feed n-hexadecane at various temperatures as a function of the sample run number over the base case 0.96 wt% Pd/H-MFI catalyst.

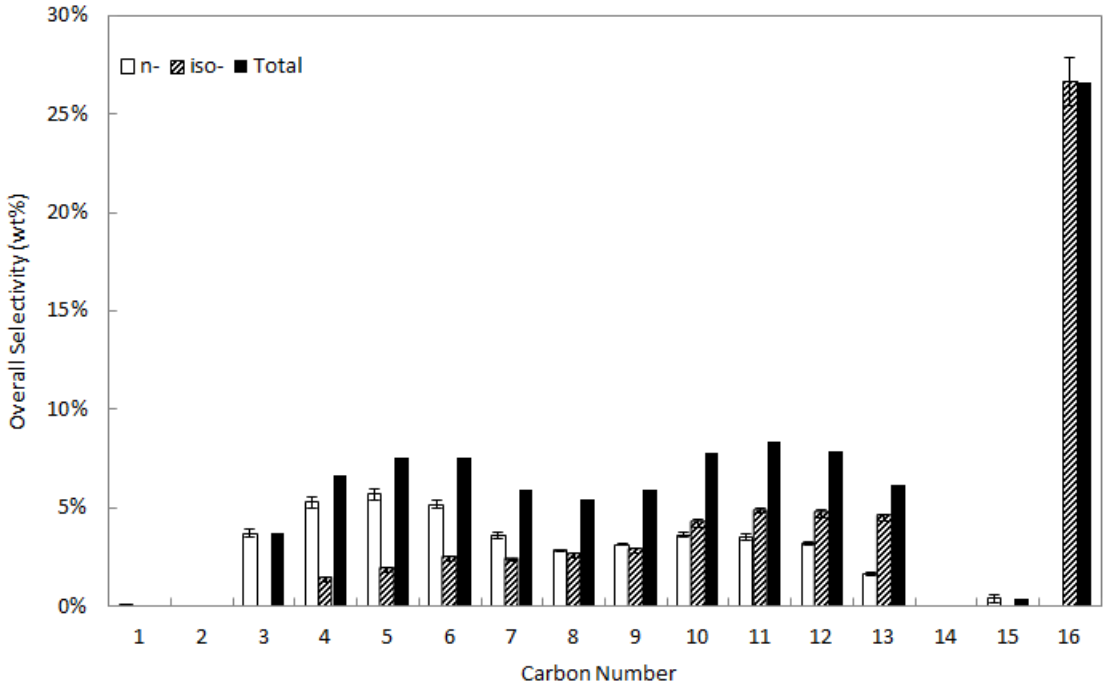

Figure 5.2: Graph of the selectivity of base case 0.96 wt% Pd/H-MFI catalyst at 215 °C and a overall n-hexadecane conversion of 16%.

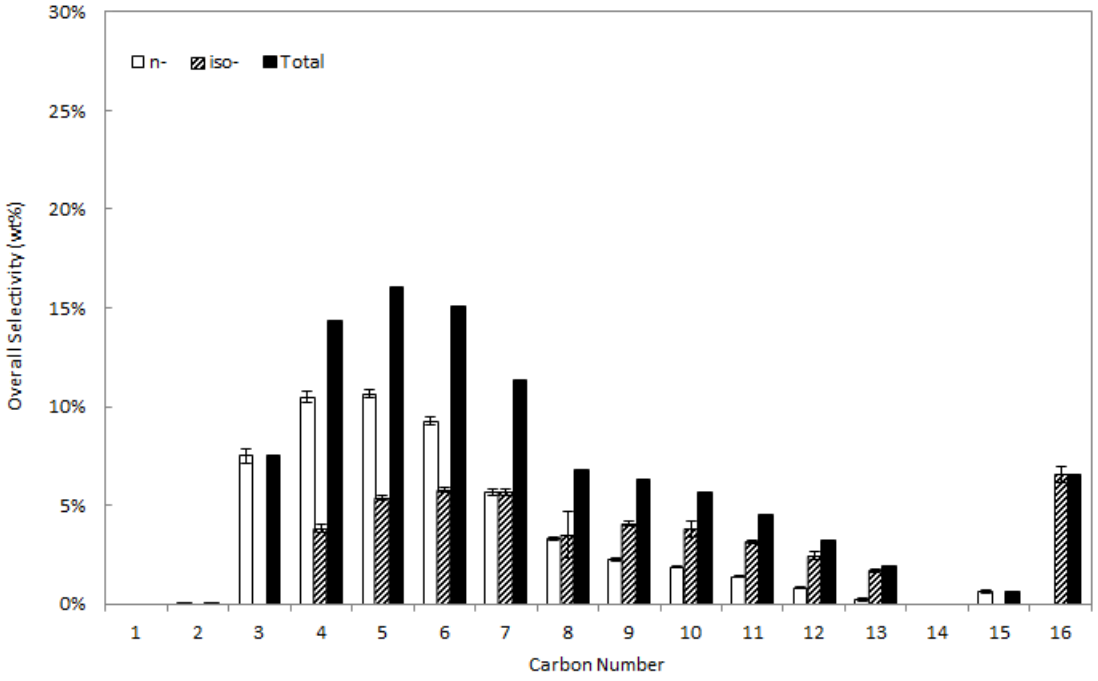

Figure 5.3: Graph of the selectivity of base case 0.96 wt% Pd/H-MFI catalyst at 240 °C and a overall n-hexadecane conversion of 91%.

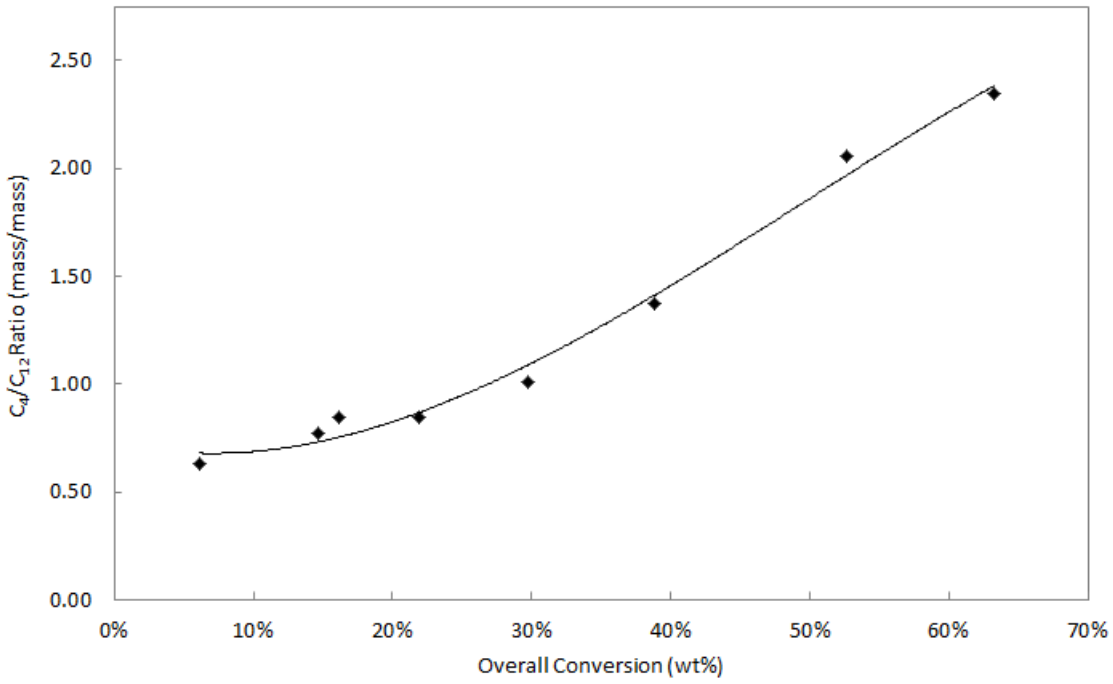

Figure 5.4: Graph of the C_4/C_{12} mass fractions as a function of overall n-hexadecane conversion for the monometallic Pd/H-MFI catalyst.

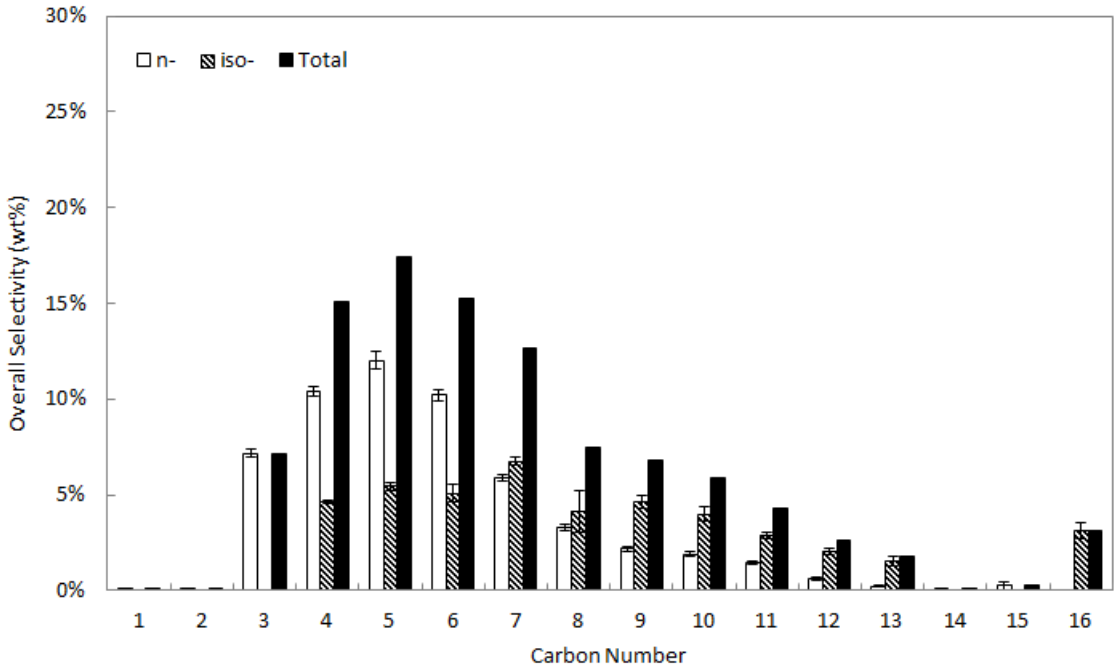

Figure 5.5: Graph of the selectivity in the presence of carbon monoxide of base case 0.96 wt% Pd/H-MFI catalyst at 225 °C and a overall n-hexadecane conversion of 40%.

5.1.2 Effect of Carbon Monoxide on Pd/H-MFI Hydrocracking Selectivity

The addition of carbon monoxide to the base case catalyst causes a dramatic increase in the light carbon fraction product selectivity resulting in a non-ideal product spectrum. This change in the product spectrum is caused by a physical change within the catalyst (i.e. migration of palladium metal sites to the external zeolite surface (Brosius and Fletcher, 2014)) which leads to the increased re-absorption of olefin compounds and thus increased secondary cracking. The product spectrum of the base case catalyst being exposed to CO can be seen in figure 5.5. This spectrum exhibits the salient features of a non-ideal catalyst as described in section 2.3.3. It also shows the significant secondary cracking present and has a C_4/C_{12} ratio of 5.72, notably higher than in the absence of CO at a similar conversion (i.e. $C_4/C_{12} = 1.37$ at 230 °C and 39% feed conversion - see figure 5.6). The minimal feed isomerization, approximately 3 wt%, is appreciably lower than in the absence of CO, approximately 24%, serves to emphasise the non-ideality of the catalyst in the presence of CO. This effect was found to be irreversible and is consistent with that of Brosius and Fletcher (2014).

5.2 Results of Bimetallic PdFe/H-MFI Catalyst Tested

5.2.1 Effect of Low Iron Loading on Selectivity and Conversion

Various loading combinations of iron and palladium were tested in order to determine whether chemical anchoring of the mobile palladium metal is possible (see section 4.1.2). The lowest loaded iron-palladium catalyst that was tested is the PdFe/H-MFI (4,24). This catalyst has the same palladium loading as the base case with a Fe/Pd_6 ratio of 1 (see table 4.1). The final C_4/C_{12} ratios at the tested conditions presented in figure 5.7 are remarkably similar to the results obtain in the base case (see figure 5.4). There is however a slight increase in the C_4/C_{12} over the entire conversion range as compared to the base case. This increase is attributed to the Fe ion acting as a nucleation and growth source for palladium during catalyst preparation causing an increase in secondary cracking.

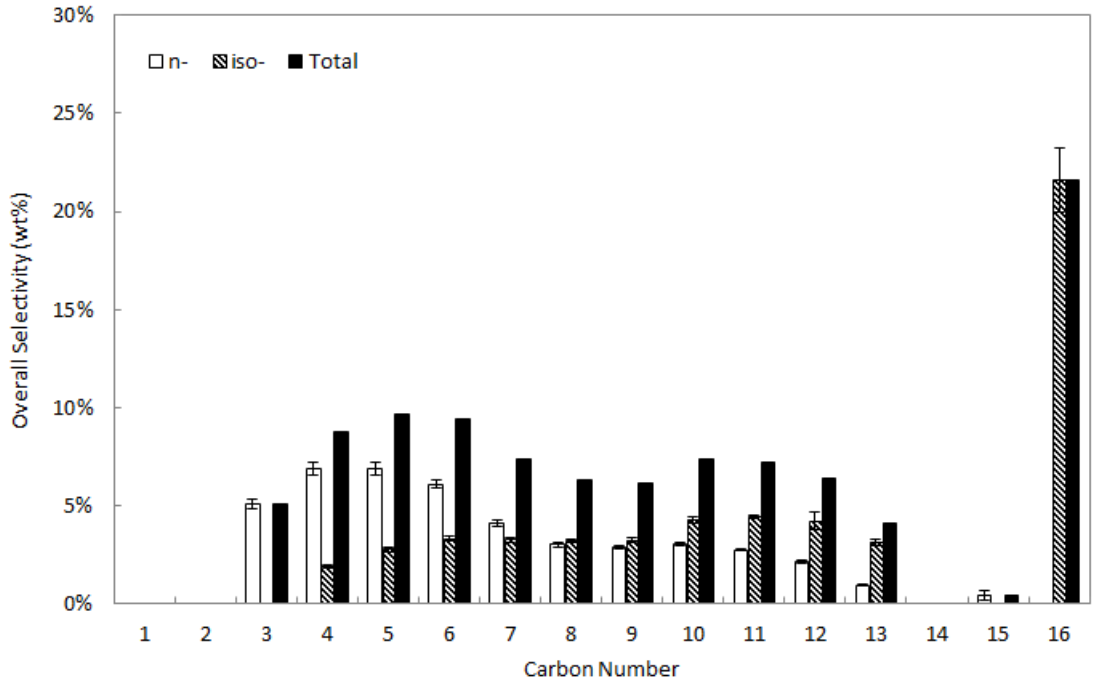

Figure 5.6: Graph of the selectivity of base case 0.96 wt% Pd/H-MFI catalyst at 230 °C and a overall n-hexadecane conversion of 40%.

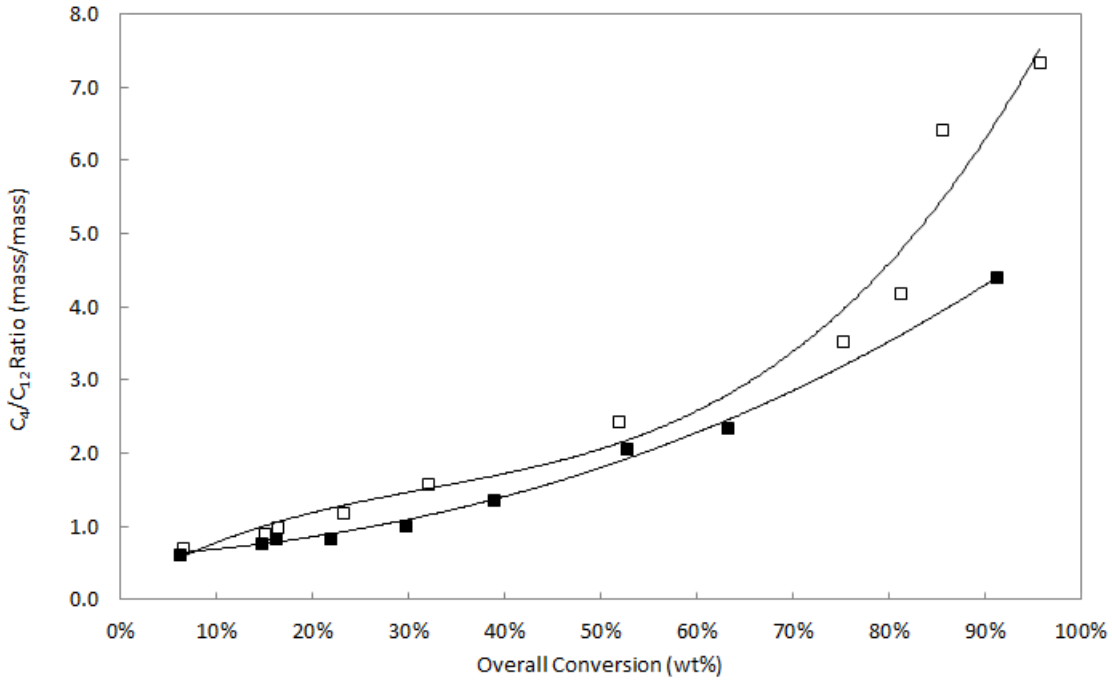

Key: (■) monometallic 0.96 wt% Pd/H-MFI; (□) bimetallic PdFe/H-MFI (4,24) with $Fe/Pd_6 = 1$.

Figure 5.7: Comparison of the C_4/C_{12} mass fractions as a function of overall n-hexadecane conversion for the monometallic Pd/H-MFI and bimetallic PdFe/H-MFI (4,24) catalysts.

5.2.2 Effect of High Iron Loading on Selectivity and Conversion

A higher loading of iron was tested in the form of a PdFe/H-MFI (4,12) and (16,12) catalyst which has Fe/Pd_6 ratio of 2 and 8 respectively. From figure 5.8 it can be seen that the carbon fraction selectivities of the bimetallic PdFe/H-MFI (4,24), PdFe/H-MFI (4,12) and PdFe/H-MFI (16,12) as well as the base case monometallic 0.96 wt% Pd/H-MFI catalyst are identical at circa 30% overall n-hexadecane conversion. These catalyst also have a similar feed isomerization conversion in the range of 20-24%.

The PdFe/H-MFI (16,12) catalyst result was taken at 215 °C while the rest were taken at 225 °C. This is consistent with the results shown in figure 2.6 as the activity of the low palladium loading catalyst is much higher.

This higher activity however does not coincide with over cracking as can be seen by the flat product distribution curve in figure 5.8. Therefore, it can be concluded that the PdFe/H-MFI (16,12) catalyst is not limited by the metal function and that a metal:acid site balance is present within the low palladium loading catalyst. This catalyst thus differs from the catalyst prepared by Brosius and Fletcher (2014) who found that significant secondary cracking is always present with low loading Pd/H-MFI catalyst.

Interestingly, when comparing the selectivity results mentioned to that of the low iron and low palladium loading catalyst, the PdFe/H-MFI (16,24), at a similar conversion (circa 30%) and temperature (220 °C) an effect of iron can be seen (see figure 5.8). At a lower palladium and iron loading it was found that the bimetallic catalyst behaves as expected of a low palladium loading monometallic catalyst i.e. identical selectivity with higher activity indicating a negligible effect of iron on the hydrocracking catalyst. The PdFe/H-MFI (16,24) catalyst exhibits significantly more secondary cracking as seen by the shift towards low carbon number fractions and a feed isomerization conversion of approximately 3%. This selectivity differs greatly from that of the PdFe/H-MFI (16,12) catalyst which has more iron.

The effect of iron can be attributed to pore blockage during catalyst preparation for high iron loadings. As the iron precursor was prepared before the addition of the active palladium metal, there exists the possibility that the iron has blocked access to the internal acid sites. These internal acid sites consequently can not be accessed during the hydrocracking reaction. The removal of these acid sites from the reaction result in a improved metal:acid ratio for the low loading palladium catalysts. At low iron loadings however the pore blockage is negligible and thus the extremely poor metal:acid site balance still exists which causes the significant secondary cracking as seen by the PdFe/H-MFI (16,24) catalyst.

In figures 5.10 and 5.11 the isomerization resemblance can be seen. These examples were chosen to illustrate the similarity between the catalyst with and without iron at a high palladium loadings as it shows the almost equivalent selectivity towards both straight chain and olefin compounds. The effect of iron pore blockage in these cases can not be seen due to the pre-existing metal:acid site balance. Therefore the removal of any internal acid sites does not affect the quasi-equilibrium between the metal and acid functions as the catalyst is already limited by the number of acid sites. As these catalyst have the same palladium weight loading and were prepared similarly, it was concluded that the addition of well dispersed iron has a negligible effect of the activity or selectivity of the catalyst at high palladium loadings.

The effect of iron can be further seen in figure 5.9 which shows the comparison between the monometallic base case 0.96 wt% Pd/H-MFI and the PdFe/H-MFI (16,12) catalyst. Over the entire conversion range tested, the PdFe/H-MFI (16,12) exhibits an improved C_4/C_{12} ratio which is lower than the base case catalyst and much lower than the C_4/C_{12} ratio of the PdFe/H-MFI (16,24) catalyst - see figure 5.12. It can therefore be concluded that if enough internal acid sites are blocked, a low loading palladium catalyst can have the same selectivity as that of the ideal 0.96 wt% Pd/H-MFI. This differs quite significantly from the results of the low iron loading which shows a negligible effect as noted in section 5.2.1. The effect of iron can thus be seen to remove the non-ideality of a low loading palladium catalyst by ensuring a metal:acid site balance.

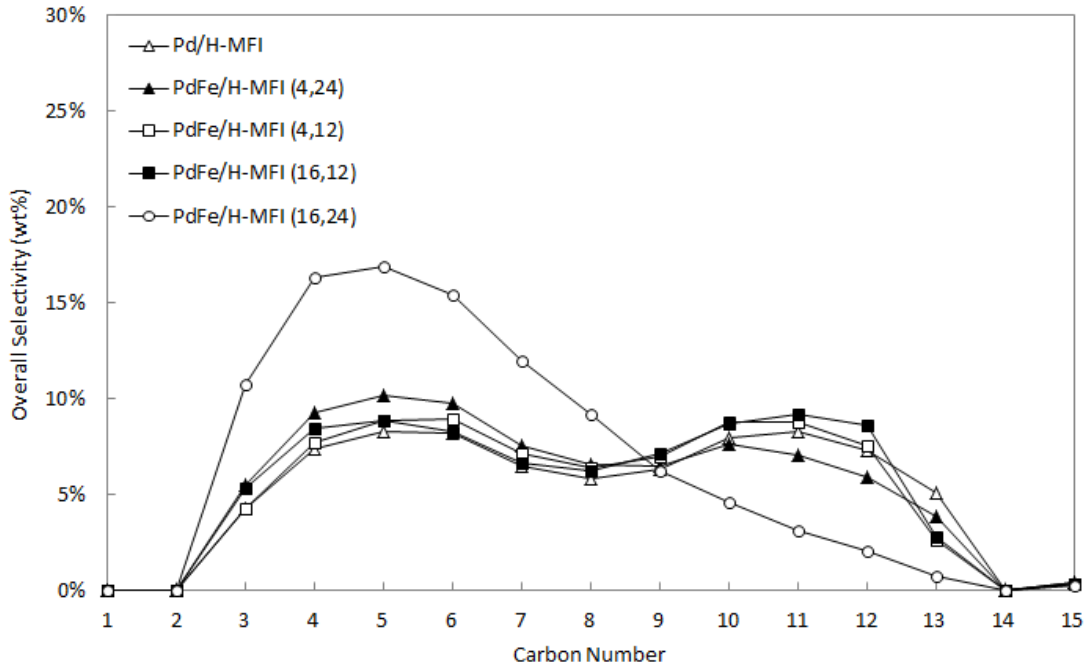

Key: (△) base case 0.96 wt% Pd/H-MFI; (▲) PdFe/H-MFI (4,24) with $Fe/Pd_6 = 1$; (□) PdFe/H-MFI (4,12) with $Fe/Pd_6 = 2$; (■) PdFe/H-MFI (16,12) with $Fe/Pd_6 = 8$; (○) PdFe/H-MFI (16,24) with $Fe/Pd_6 = 4$.

Figure 5.8: Correlation between total carbon fraction selectivities of 0.96 wt% Pd/H-MFI with various iron loadings at 215-225°C and an overall n-hexadecane conversion of circa 30%.

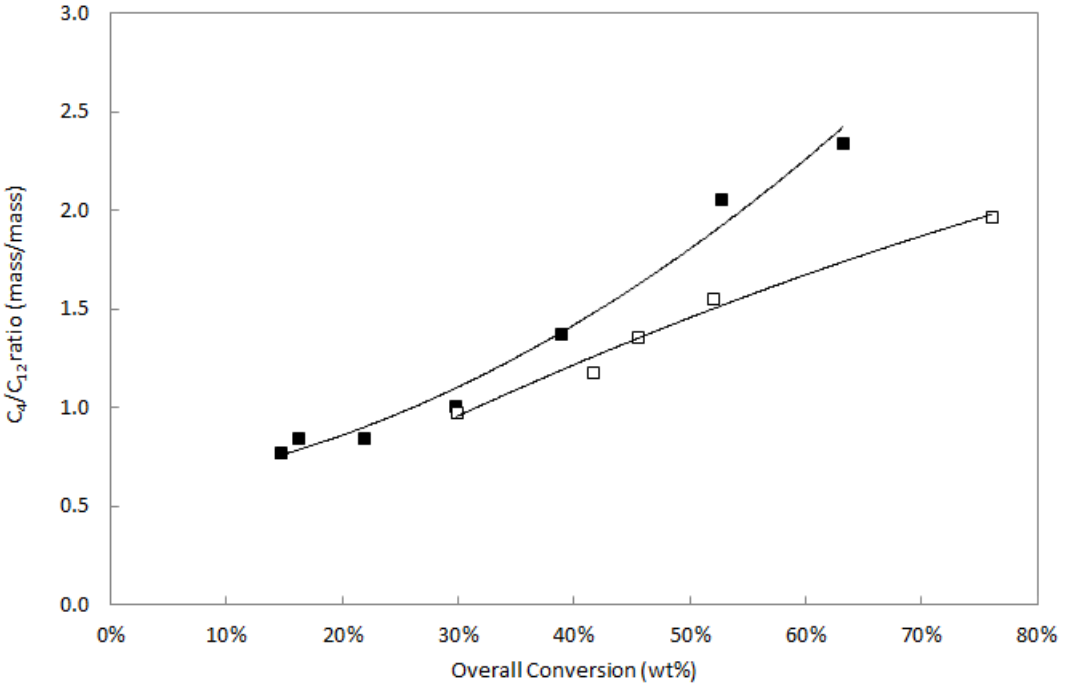

Key: (■) monometallic base case 0.96 wt% Pd/H-MFI; (□) bimetallic PdFe/H-MFI (16,12) with $Fe/Pd_6 = 8$.

Figure 5.9: Comparison of the C_4/C_{12} mass fractions as a function of overall n-hexadecane conversion for the monometallic Pd/H-MFI and bimetallic PdFe/H-MFI (16,12) catalysts.

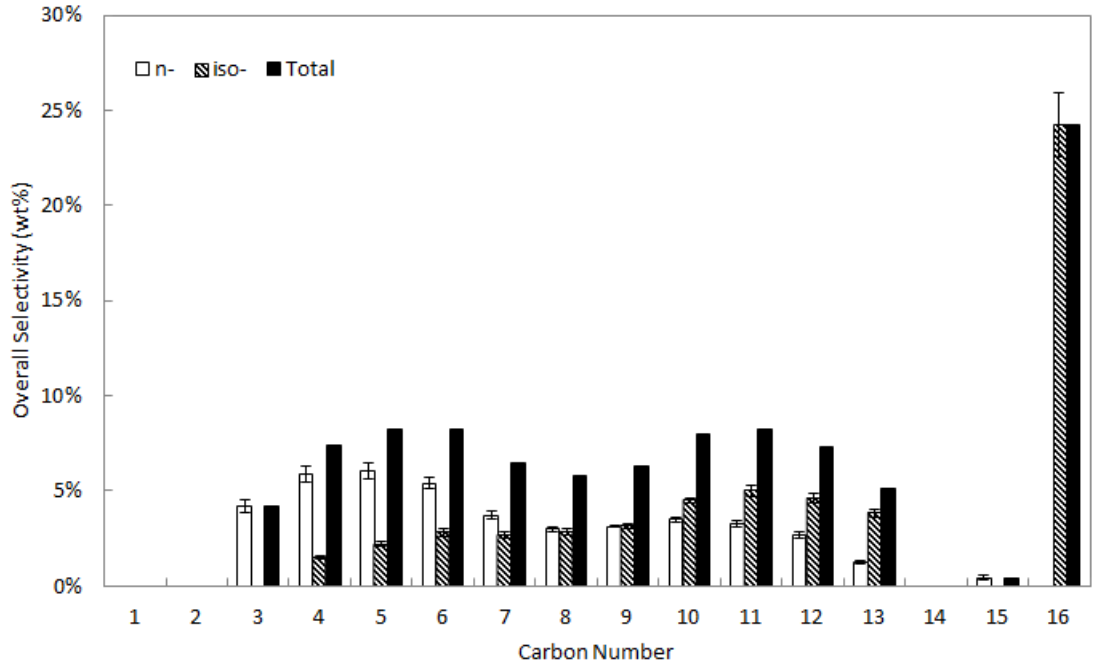

Figure 5.10: Graph of the selectivity of base case 0.96 wt% Pd/H-MFI catalyst at 225 °C and a overall n-hexadecane conversion of 30%.

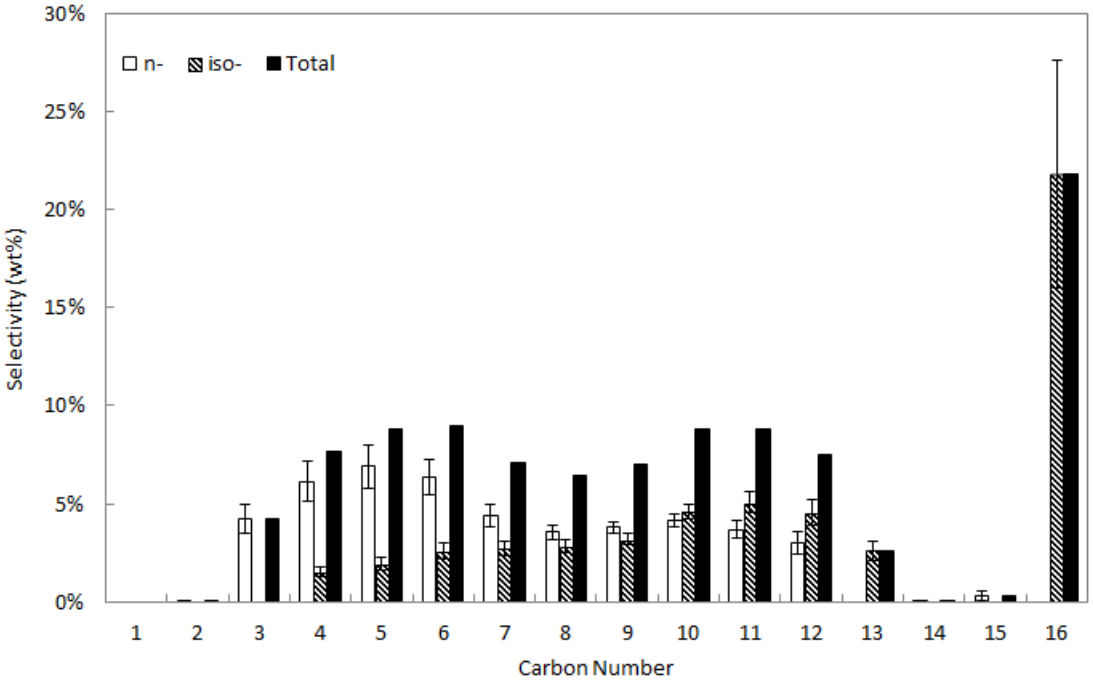

Figure 5.11: Graph of the selectivity of PdFe/H-MFI (4,12) catalyst at 225 °C and a overall n-hexadecane conversion of 31%.

5.2.3 Effect of Palladium Loading on Selectivity and Conversion

As noted in section 5.2.1, the effect of iron is negligible at low iron loadings. As such a comparison of the base case catalyst may be done with that of a bimetallic catalyst, ignoring the presence of iron in the absence of CO for the low iron loading. The effect of palladium loading can be seen in figure 5.12 which compares the C_4/C_{12} ratio of the PdFe/H-MFI (16,24) and the base case Pd/H-MFI catalyst.

The low palladium loaded catalyst can be seen to have notably larger C_4/C_{12} ratio over the entire conversion range when compared to the base case catalyst. This is due to the inherent imbalance of the metal:acid sites ratio within the catalyst. The metal:acid imbalance means that the low palladium loaded catalyst is limited by the metal function due to the low number of metal sites available. As a result of this the olefin product intermediates are not able to access a metal site to be hydrogenated and are further cracked (Brosius and Fletcher, 2014). The behaviour of the low palladium and low iron loaded catalyst, PdFe/H-MFI (16,24), is similar to that of a low loading monometallic catalyst, 0.16 wt% Pd/H-MFI, which further demonstrates the negligible iron effect at low iron loadings as found in section 5.2.1.

The results from the catalyst containing the 0.48 wt% palladium proved to be inconclusive due to a hydrogen gas manifold supply problem. The change in the hydrogen pressure negatively affected the mass flow controller supply causing scattered conversion readings. Once the problem was alleviated, the conversion did not stabilize and therefore the experiment was abandoned. Readings up to 30% conversion were taken before the supply problem and the data were found to be similar to that of the high loading catalyst. This is in accord with figure 2.6, as the activity of the 0.48 wt% catalyst is similar to that of the 0.96 wt% catalyst. Further testing was thus deemed unnecessary.

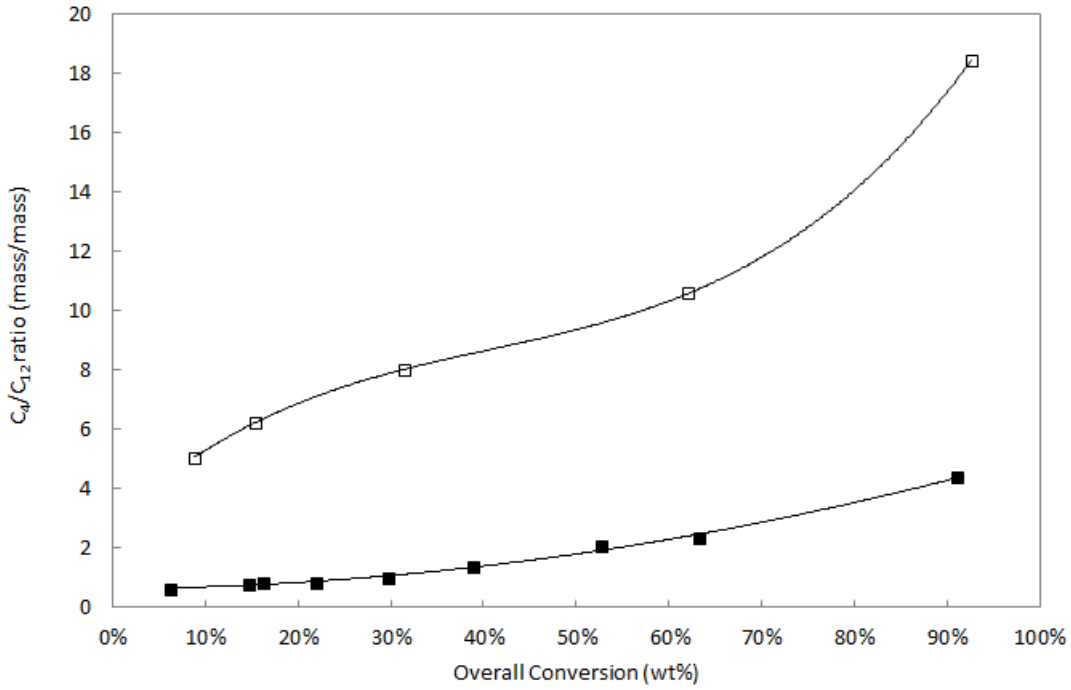

Key: (□) 0.16 wt% palladium loading in PdFe/H-MFI (16,24); (■) 0.96 wt% palladium loading in Pd/H-MFI.

Figure 5.12: Graph of the C_4/C_{12} mass fractions for 0.96 wt% and 0.16 wt% palladium loaded catalyst as a function of overall n-hexadecane conversion.

5.2.4 Effect of Water on PdFe/H-MFI Catalysts

As water is a co-product of the low temperature Fischer-Tropsch synthesis, its effect on the hydrocracking catalyst conversion and selectivity was tested. Water was co-fed into the reactor using a flow rate equal to that of an 80% FT reaction conversion (assuming 100% selectivity towards the feed n-hexadecane). This corresponded to a flow rate of 0.01 ml/min using the given conditions set out in section 4.3. The results of the H_2O testing can be seen in figures 5.13 - 5.15 which show a number of key features and similarities.

The main similarity between the catalyst in the presence versus in the absence of water is the shape of the overall conversion curve in figure 5.13. The presence of water merely shifts the curve by approximately 30 °C. This shift however is accompanied by a sizeable increase in feed isomerization which indicates that ideal hydrocracking may be achieved at high conversions i.e. the presence of a large fraction of iso-C_{16} is an indication of the presence of a large olefin supply for β-scission - see bimetallic mechanism in figure 2.4. It is also noted here that there is a maximum feed isomerization of approximately 30% in the absence of water while in the presence of water almost complete feed isomerization can be achieved at low conversions.

Further evidence of enhanced ideal hydrocracking in the presence of water can be seen by comparing figures 5.14 and 5.15. The outstanding difference here is that of the feed isomerization which in the presence of water is inflated to 58%, approximately 20% greater than without water. This trend is not limited to feed products as the isomerization product fraction increases throughout the carbon number range.

While in the absence of water, the catalyst does perform ideally - C_4/C_{12} ratio of 0.89, the addition of water further improves the selectivity - C_4/C_{12} ratio of 0.56. This opens up the possibility of pure primary cracking on an H-MFI catalyst.

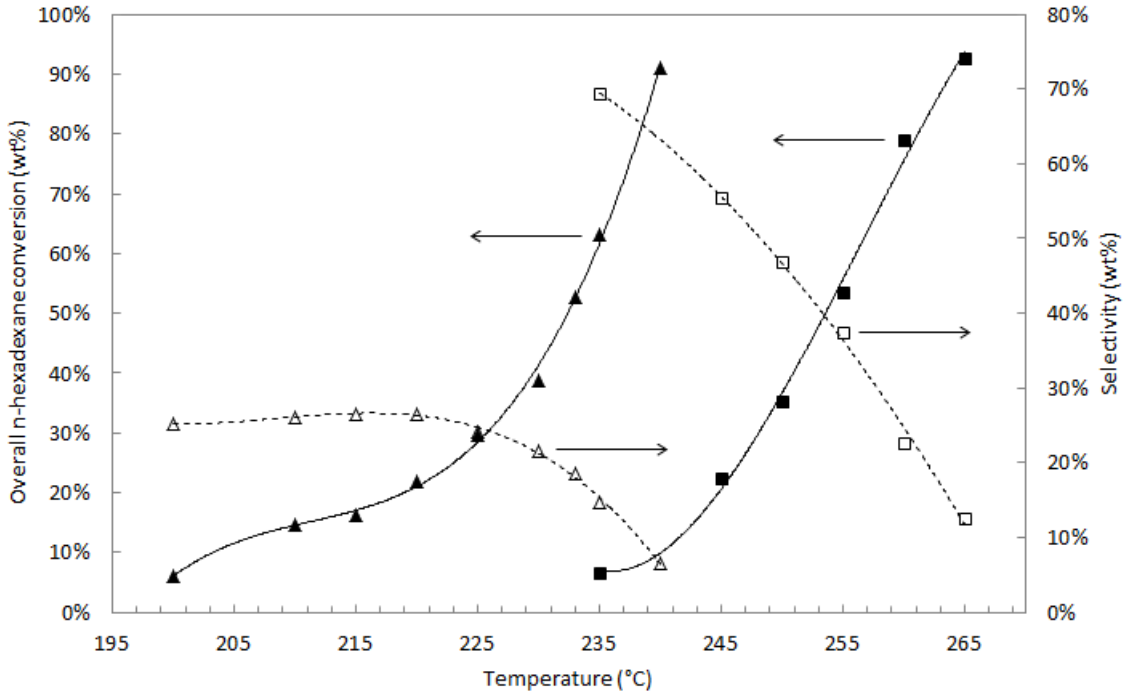

Key: (▲) Conversion as a function of temperature in the absence of H_2O; (■) Conversion as a function of temperature for 0.96 wt% palladium catalyst in the presence of H_2O; (△) iso-C_{16} fraction selectivity in the absence of H_2O; (□) iso-C_{16} fraction selectivity in the presence of H_2O.

Figure 5.13: Graph of the conversion and selectivity towards feed isomerization mass fraction for 0.96 wt% palladium loaded catalyst as a function of reaction temperature.

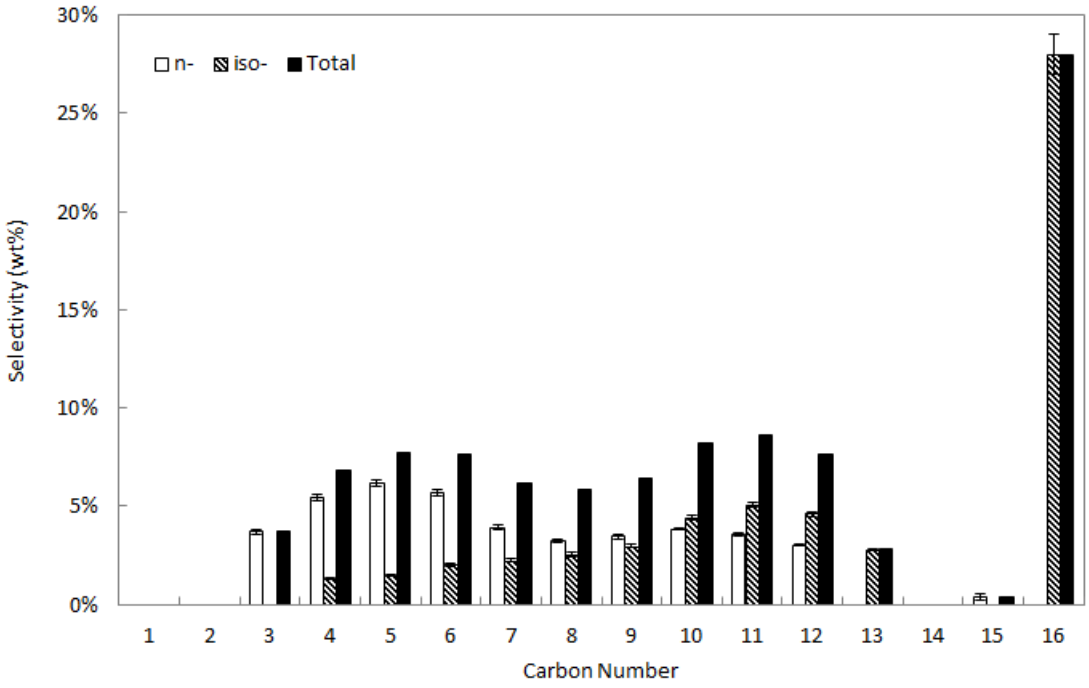

Figure 5.14: Graph of the selectivity of PdFe/H-MFI (4,24) catalyst at an overall n-hexadecane conversion of 24%.

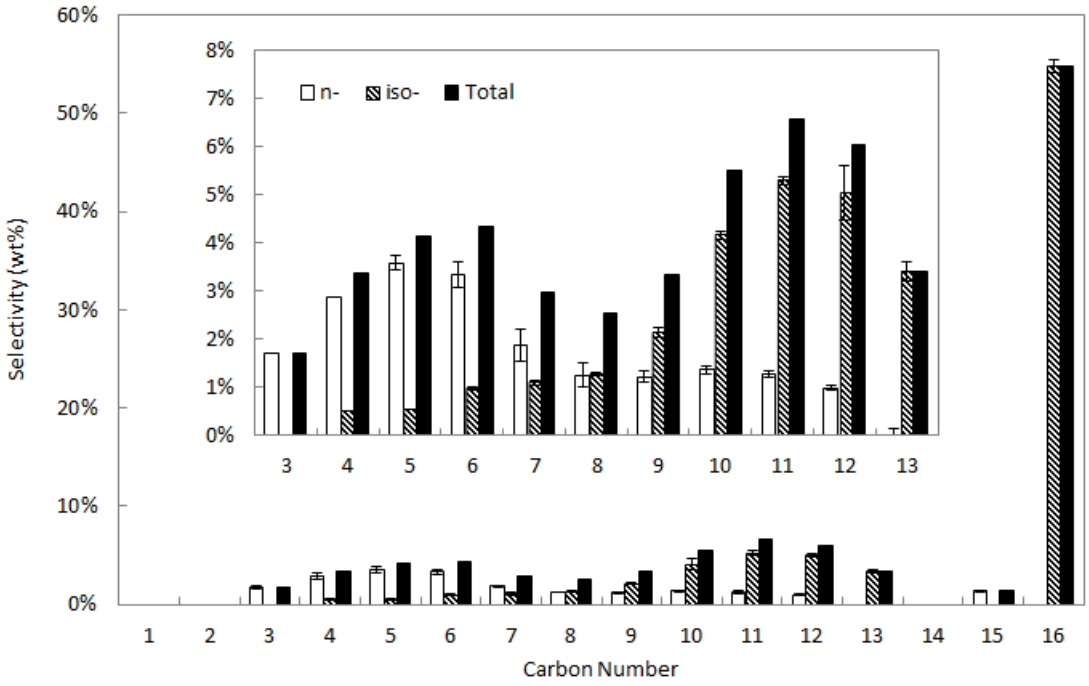

Figure 5.15: Graph of the selectivity of PdFe/H-MFI (4,24) catalyst at an overall n-hexadecane conversion of 22% in the presence of H_2O.

5.2.5 Carbon Monoxide Tolerance of PdFe/H-MFI Catalysts

The main aim of this project is to determine whether at a specific ratio of iron to palladium a bimetallic PdFe/H-MFI catalyst will be tolerant to CO. The results shown in figure 5.16 indicate that this is not the case at the tested loading ratios. The results presented are given for the various Fe/Pd_6 ratios as well as the base case catalyst.

It can be seen that the addition of iron using the solid-state ion exchange method described in section 4.1.3 is unsuitable for the chemical anchoring of palladium in a bimetallic PdFe/H-MFI hydrocracking catalyst. In the presence of CO, all the tested bimetallic catalysts show a dramatic shift towards lower carbon fractions due to secondary cracking analogous to that of the monometallic catalyst behaviour. It was thus concluded that palladium metal is still highly mobile in the bimetallic catalyst in the presence of CO.

It was found that the addition of water did not alleviate the problem of the imbalance between metal and acid functions in any of the cases. It is thus thought that the CO not only causes a migration of the palladium to the external surface but also poisons the majority of the metal sites resulting in an extremely low amount of active metal. This in turns means that even with the deactivation of acid sites by water, the metal and acid function balance can not restored at the given metal loading.

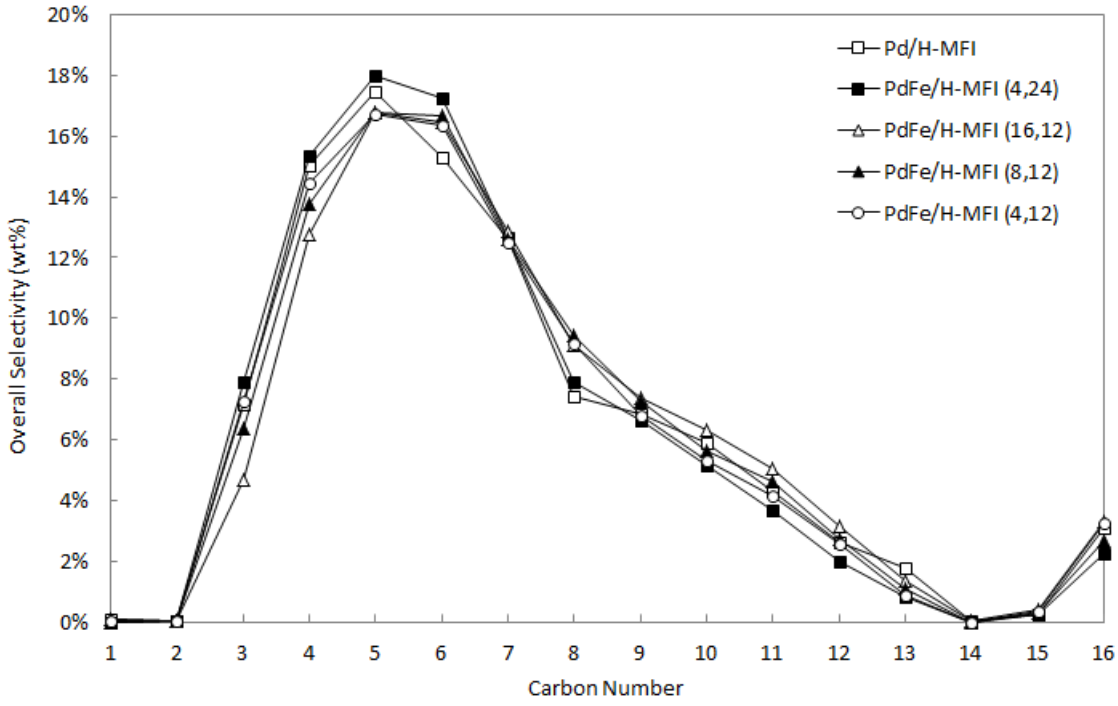

Key: (□) 0.96 wt% Pd/H-MFI; (■) PdFe/H-MFI (4,24) with $Fe/Pd_6 = 1$; (△) PdFe/H-MFI (16,12) with $Fe/Pd_6 = 8$;(▲) PdFe/H-MFI (8,12) with $Fe/Pd_6 = 4$;(○) PdFe/H-MFI (4,12) with $Fe/Pd_6 = 2$.

Figure 5.16: Overall selectivity of the monometallic Pd/H-MFI and various bimetallic PdFe/H-MFI catalysts in the presence of CO after approximately 24 hours.

Chapter 6

Discussion

"It was my intention to present you with a problem only after I had found an appropriate solution."
Klaus Mikaelson - The Originals

6.1 Effect of Iron and Palladium Loading on PdFe/H-MFI Catalyst

The effect of iron loading in the absence of CO was determined using the base case monometallic 0.96 wt% Pd/H-MFI as well as the bimetallic PdFe/H-MFI (4,24), (4,12), (16,24), (16,12) which have a Fe/Pd_6 ratio of 1, 2, 4 and 8 respectively. The activity of the high palladium loaded catalysts i.e. PdFe/H-MFI (4,24) and (4,12) was found to be identical to that of the base case catalyst indicating no effect of iron in terms of overall activity for high palladium loaded catalysts.

The PdFe/H-MFI (16,24) catalyst was found to have a higher activity than the other bimetallic catalyst and behaved similarly to that of the low loaded monometallic palladium catalyst showed by Brosius and Fletcher (2013). This increase in activity is due to the lifting of mass transfer restrictions within the zeolite (Brosius and Fletcher, 2014). At high metal loadings the rate of hydrocarbon transport is limited due to the presence of a large amount of metal within the catalyst. At low loadings, this restriction is lifted resulting in an increased activity. This result confirmed the negligible effect of low loaded iron on the overall activity. The reason for this may be that there is no interaction between the palladium and iron particles i.e. they are too far apart; they simply do not alloy or that the iron particles play no part in the reaction.

It was found that at low iron loadings the selectivity shifts slightly towards lower carbon fractions. This supported the latter conclusion as it is thought that at low iron loadings the iron acts as a nucleation source for palladium during preparation. This results in lower dispersion and larger palladium particles. As the Pd loading is the same, the size increase in Pd particles causes an increased distance between acid and metal sites allowing for an increased rate of olefinic intermediary product adsorption and secondary cracking.

The result of the PdFe/H-MFI (16,12) did however show a positive effect of iron. The catalyst was found to have a much lower C_4/C_{12} ratio when compared to the low iron low palladium catalyst, PdFe/H-MFI (16,24). The C_4/C_{12} ratio of PdFe/H-MFI (16,12) was also noted to be even better than the ideal base case catalyst. This effect of iron was attributed to pore blockage during the Fe/H-MFI precursor preparation. For a low palladium loaded H-MFI catalyst the amount of metal sites available for de-/hydrogenation is low meaning that there is an inherently poor metal:acid site ratio. As the addition of iron to the zeolite was done before the impregnation with palladium, it is theorized that for high loadings of iron, the internal acid sites of the zeolite are blocked by iron particles. As a result of this the internal acid sites are essentially removed from the hydrocracking reaction leaving the catalyst with an improved metal:acid site balance. This effect is not seen in a catalyst with a high palladium loading as the metal:acid site balance already exists.

6.2 Effect of Water on PdFe/H-MFI Catalyst

The addition of water to the hydrocracking reaction has a promotional effect on the overall selectivity of the PdFe/H-MFI catalysts. It was found that the overall conversion range is approximately 30 °C higher than without water. This shift in conversion is coupled with a remarkable change in the feed isomerization selectivity. In the absence of water the overall feed isomerization was limited to 30% due to the number of acid sites (total acidity) i.e. the large number of acid sites present ensured that the feed isomerization could not exceed this value. In the presence of water however this limitation is lifted due to the deactivation of the acid sites. This results in an enhanced metal:acid function balance. Notably, these results were found to be fully reversible upon the removal of water.

As a consequence of this improved balance the overall selectivity was shifted towards almost pure primary cracking at low conversions due to the increase in intermediary olefinic and carbenium ion compounds present. Consequently an increase in the various carbon number isomerization fractions was noted and attributed to the increased possibility of alkyl and hydride shift reactions i.e. as more olefins are present, there is an increased chance of branching.

Yan (1972) noted that the promotional effect of water may be explained by either water deactivating the catalyst by competing with hydrocarbons for the surface or by hydrating protons present in the catalyst by diminishing acid strength. This suggests that within the H-MFI catalyst either the total acid strength or the number of acid sites present have a negative effect on the possibility of pure primary cracking (see section 2.3.2). It can thus be concluded that while the H-MFI zeolite achieved the best results when tested by Kukard (2008), there exists a possibility that the zeolite can be altered to ensure an even better selectivity. Occelli (2010) noted an increase in Si/Al resulted in decreasing total acidity for MFI catalysts. Therefore lowering the number of zeolite acid sites through dealumination without an increase in total acidic strength could result in an enhanced metal:acid function balance and thus an improved H-MFI catalyst.

6.3 Carbon Monoxide Tolerance of PdFe/H-MFI Catalysts

The results presented in section 5.2.5 were taken after 24 hours of co-feeding CO as to illustrate the effect of CO on the bimetallic catalyst over a suitable time frame. While at this stage all of the catalysts were still deactivating, continuing the experiments were deemed unnecessary as the results were clear. With the addition of CO the activity of all the catalysts showed a marked increase due to the migration of the palladium and consequently removal of mass transfer limitations within the catalyst. This behaviour of the bimetallic catalyst mimicked that of the monometallic catalyst inferring a negligible iron effect. As a result it can be concluded that the preparation method did not allow for the chemical anchoring as proposed in section 2.5.2.

The removal of active metal sites through particle growth is thought to be coupled with that of CO poisoning due to the inability to restore the catalyst metal:acid function balance by the addition of water. The increase in the feed isomerization caused by the addition of water was found to be insufficient as the PdFe/H-MFI catalysts retained the low feed isomerization rate in the presence of CO. As the selectivity towards feed isomerization is indicative of the quasi-equilibrium between the hydrogenation/dehydrogenation reactions (Bouchy et al., 2009) it was concluded that even with the addition of water the catalyst remains limited by the metal function. This can be seen by the low iso-C_{16} fraction obtained in the combined presence of CO and water. It is therefore concluded that the bimetallic PdFe/H-MFI catalyst prepared through solid state ion exchange and incipient wetness impregnation exhibits no noticeable carbon monoxide tolerance when compared to a monometallic Pd/H-MFI catalyst.

Chapter 7
Conclusions and Recommendations

"Leonard, prepare to be humbled and weep at the glory of my genius."
Dr Sheldon Cooper - The Big Bang Theory

7.1 Suitability of Bimetallic PdFe/H-MFI for Hydrocracking at Low Temperature Fischer-Tropsch Conditions

The key aim of this project was to find a suitable bimetallic catalyst for wax hydrocracking under Fischer-Tropsch conditions. From previous works and literature it was suggested that the use of a chemically anchored (by iron) palladium on support H/MFI (i.e. PdFe/H-MFI) catalyst may be appropriate in obtaining the objective of an active and selective catalyst that is tolerant to the effects of carbon monoxide.

However, the results of this project show that this is not the case when the catalyst is prepared through the use of the solid-state ion exchange method for adding iron to H-MFI followed by palladium incipient wetness impregnation. The bimetallic PdFe/H-MFI catalysts prepared in this manner do not show any tolerance to carbon monoxide. It is thought that this is due to the minimal interaction between the iron and palladium particle resulting in iron playing no part in the hydrocracking reaction. As such the results from the tested bimetallic catalyst were found to be near identical to that of the monometallic Pd/H-MFI catalyst in that the palladium metal migrated and clustered on the external zeolite surface causing severe secondary cracking in the presence of CO. The root cause of the secondary cracking is the imbalance between the HD/DHD and acid functions due to the lack of metal sites available after migration.

A study into the effect of water on the activity and selectivity of the tested catalyst revealed that almost pure primary cracking is possible on the H-MFI catalysts. Water was seen to reversibly deactivate the acid function causing an decrease in the selectivity towards undesired low carbon fractions. This indicated that the total acidity of the H-MFI catalyst may be too high and that if further dealuminated, the catalyst selectivity may be improved due to an enhanced metal to acid site balance. This would however lower the cetane number of the desired diesel product in an industrial case due to the increase in the isomerization fractions.

Considering that the carbon monoxide addition causes the removal of HD/DHD sites and the addition of water deactivates the acid sites, it was thought that the balance could be restored when both carbon monoxide and water were added. It was found however that the CO addition effect (thought to be due to the added effect of poisoning as well as metal migration) was significantly greater than that of water and thus the balance could not be re-established.

For further studies it is suggested that different methods be used for the chemical anchoring in the preparation of PdFe/zeolite catalyst (e.g. rotary evaporation ion exchange under vacuum (Elangovan et al., 2002) or chemical vapour deposition (He et al., 2009) and that the support H-MFI total acidity be reduced to obtain the enhanced metal acid site balance found. It is also suggested that as a secondary option, the palladium loading be increased to offset its migratory nature in the presence of carbon monoxide.

References

Auerbach, S., Carrado, K., and Dutta, P. (2003). *Handbook of Zeolite Science and Technology*. Taylor & Francis.

Baerlocher, C. and McCusker, L. (2013). Database of Zeolite Structures - Framework Type MFI (Material: ZSM-5).
Available: http://www.iza-structure.org/databases.
Last Accessed: 19 August 2014.

Bekkum, H. v., Jansen, J., and Flanigen, E. (1991). *Introduction to zeolite science and practice*. Elsevier.

Bouchy, C., Hastoy, G., Guillon, E., and Martens, J. A. (2009). Fischer-Tropsch waxes upgrading via hydrocracking and selective hydroisomerization. *Oil & Gas Science and Technology-Revue de l'IFP*, 64(1):91–112.

BP (2013). BP statistical review of world energy.
Available: http://www.bp.com/content/dam/bp/pdf/statistical-review/statistical_review_of_world_energy_2013.pdf.
Last Accessed: 16 July 2014.

BP (2014). BP Energy Outlook 2035.
Available: http://www.bp.com/content/dam/bp/pdf/Energy-economics/Energy-Outlook/Energy_Outlook_2035_booklet.pdf.
Last Accessed: 16 July 2014.

Brosius, R. and Fletcher, J. C. Q. (2013). PGM Catalysts for Middle Distillate Fuels Production from Non-Petroleum Feedstock. *Unpublished*. University of Cape Town.

Brosius, R. and Fletcher, J. C. Q. (2014). Hydrocracking under Fischer–Tropsch conditions; the effect of CO on the mass transfer resistance by metal clusters. *Journal of Catalysis*, 317:318–325.

Choudhary, N. and Saraf, D. (1975). Hydrocracking: A review. *Industrial & Engineering Chemistry Product Research and Development*, 14(2):74–83.

Csicsery, S. M. (1984). Shape-selective catalysis in zeolites. *Zeolites*, 4(3):202–213.

Dry, M. E. (1990). The Fischer-Tropsch Process-commercial aspects. *Catalysis Today*, 6(3):183–206.

Dry, M. E. (1996). Practical and theoretical aspects of the catalytic Fischer-Tropsch process. *Applied Catalysis A: General*, 138(2):319–344.

Dry, M. E. (2001). High quality diesel via the Fischer-Tropsch process-a review. *Journal of Chemical Technology and Biotechnology*, 77(1):43–50.

Dry, M. E. (2002). The Fischer-Tropsch process: 1950-2000. *Catalysis today*, 71(3):227–241.

Elangovan, S., Bischof, C., and Hartmann, M. (2002). Isomerization and Hydrocracking of n-Decane over Bimetallic Pt-Pd Clusters Supported on Mesoporous MCM-41 Catalysts. *Catalysis letters*, 80(1-2):35–40.

Fahim, M., Al-Sahhaf, T., and Elkilani, A. (2009). *Fundamentals of Petroleum Refining*. Elsevier Science.

Fukuoka, A., Kimura, T., Kosugi, N., Kuroda, H., Minai, Y., Sakai, Y., Tominaga, T., and Ichikawa, M. (1990). Bimetallic promotion of alcohol production in CO hydrogenation and olefin hydroformylation on RhFe, PtFe, PdFe, and IrFe cluster-derived catalysts. *Journal of Catalysis*, 126(2):434–450.

Garten, R. (1976). Direct evidence for bimetallic clusters. *Journal of Catalysis*, 43(1):18–33.

Goodger, E. M. (2001). *Transport Fuels Technology: Mobility for the Millennium*. Landfall Press.

Green, D. W. et al. (2008). *Perry's chemical engineers' handbook*, volume 796. McGraw-hill New York.

Hagen, J. (1999). *Industrial Catalysis: A Practical Approach*. Wiley-Vch Weinheim.

He, N., Li, P., Zhou, Y., Ren, W., Fan, S., and Verkhozina, V. (2009). Catalytic dechlorination of polychlorinated biphenyls in soil by palladium–iron bimetallic catalyst. *Journal of hazardous materials*, 164(1):126–132.

Koen, M. and Manan, F. (2012). Bimetallic Noble Metal Loaded Zeolites for Combining Fisher-Tropsch Synthesis and Wax Hydrocracking. BSc. Honours Thesis, University of Cape Town.

Kögel, M., Mönnig, R., Schwieger, W., Tissler, A., and Turek, T. (1999). Simultaneous Catalytic Removal of NO and N_2O using Fe–MFI. *Journal of Catalysis*, 182(2):470–478.

Kukard, R. (2008). The Effect of Zeolite Type on the Hydrocracking of Long n-Paraffins. Msc. thesis, University of Cape Town.

Leckel, D. and Liwanga-Ehumbu, M. (2006). Diesel-selective hydrocracking of an iron-based Fischer-Tropsch wax fraction (C_{15}-C_{45}) using a MoO_3-modified noble metal catalyst. *Energy & Fuels*, 20(6):2330–2336.

Martens, J. and Jacobs, P. (2001). Introduction to acid catalysis with zeolites in hydrocarbon reactions. *Studies in Surface Science and Catalysis*, 137:633–671.

Occelli, M. (2010). *Advances in Fluid Catalytic Cracking: Testing, Characterization, and Environmental Regulations*. Chemical Industries. Taylor & Francis.

Okumura, K., Yoshimoto, R., Uruga, T., Tanida, H., Kato, K., Yokota, S., and Niwa, M. (2004). Energy-dispersive XAFS studies on the spontaneous dispersion of PdO and the formation of stable Pd clusters in zeolites. *The Journal of Physical Chemistry B*, 108(20):6250–6255.

Owen, K. and Coley, T. (1995). *Automotive Fuels Reference Book*. Society of Automotive Engineers, Inc., 2nd edition.

Philippaerts, A., Paulussen, S., Turner, S., Lebedev, O. I., Van Tendeloo, G., Poelman, H., Bulut, M., De Clippel, F., Smeets, P., Sels, B., et al. (2010). Selectivity in sorption and hydrogenation of methyl oleate and elaidate on mfi zeolites. *Journal of Catalysis*, 270(1):172–184.

Ray Chaudhuri, U., Chaudhuri, U. R., Datta, S., and Sanyal, S. K. (1995). Mild hydrocracking—a state of the art. *Fuel Science & Technology International*, 13(9):1199–1213.

Sasol (2013). Annual Integrated Report.
Available: http://www.sasol.co.za/sites/default/files/publications/integrated_reports/downloads/Sasol%20IR%202013lores.pdf.
Last Accessed: 21 July 2014.

Scherzer, J. and Gruia, A. J. (1996). *Hydrocracking Science and Technology*. CRC Press.

Schulz, H. (1999). Short history and present trends of Fischer-Tropsch synthesis. *Applied Catalysis A: General*, 186(1):3–12.

Shell (2014). Pearl GTL.
Available: http://www.shell.com/global/aboutshell/major-projects-2/pearl.html.
Last Accessed: 21 July 2014.

Speight, J. G. and Ozum, B. (2001). *Petroleum Refining Processes*. CRC Press.

Szostak, R. (1992). *Handbook Of Molecular Sieves: Structures*. Springer.

Tasaka, K., Tanaka, Y., and Iwama, M. (2012). Hydrocracking process and process for producing hydrocarbon oil. US Patent Publication Number US20120232172 A1.

Thybaut, J. W., Laxmi Narasimhan, C., Denayer, J. F., Baron, G. V., Jacobs, P. A., Martens, J., and Marin, G. B. (2005). Acid-Metal balance of a Hydrocracking Catalyst: Ideal versus Nonideal Behavior. *Industrial & engineering chemistry research*, 44(14):5159–5169.

Tzou, M., Jiang, H., and Sachtler, W. (1986). Chemical anchoring of platinum in zeolites. *Applied catalysis*, 20(1):231–238.

Valavarasu, G., Bhaskar, M., and Balaraman, K. (2003). Mild hydrocracking - a review of the process, catalysts, reactions, kinetics, and advantages. *Petroleum science and technology*, 21(7-8):1185–1205.

Weitkamp, J. (2000). Zeolites and catalysis. *Solid State Ionics*, 131(1):175–188.

Weitkamp, J. (2012). Catalytic Hydrocracking - Mechanisms and Versatility of the Process. *ChemCatChem*, 4(3):292–306.

Weitkamp, J., Jacobs, P. A., and Martens, J. A. (1983). Isomerization and hydrocracking of C_9 through C_{16} n-alkanes on Pt/HZSM-5 zeolite. *Applied Catalysis*, 8(1):123 – 141.

Weitkamp, J. and Puppe, L. (1999). *Catalysis and Zeolites: Fundamentals and Applications*. Springer.

Wen, B., Jia, J., and Sachtler, W. M. (2002). Chemical anchoring of palladium by Fe oxo ions in zeolite ZSM-5. *The Journal of Physical Chemistry B*, 106(30):7520–7523.

Xu, L., Lei, G.-D., and Sachtler, W. M. H. (1993). Formation of PdFe Alloy Clusters in Zeolite Y. *The Journal of Physical Chemistry*, 97(44):11517–11523.

Yan, T. (1972). The promotional effect of water in hydrocracking. *Journal of Catalysis*, 25(2):204–211.

Appendix A
Temperature Profiles

This appendix outlines the procedure and results of the reactor temperature profile. The reactor temperature is controlled by the use of four individual temperature controllers which heat four adjacent heating blocks (i.e. one temperature per each heating block). As these blocks are adjacent to each other, there is significant heat transfer and as such the set point temperature is not equal to the actual temperature in the reactor. An accurate temperature profile was therefore needed before any testing could take place.

Determining the Reactor Isothermal Zone

The temperature profile was achieved through the use of a K-type thermocouple which was inserted into the thermowell that runs through the length of the reactor. The temperature measurement was taken on a Gefran 600 temperature controller. Starting from the bottom of the reactor, the thermocouple tip (i.e. the point at which the temperature measurement is taken) was raised by 1 cm for each new reading. This allowed for an exact measurement of the temperature at each point in the reactor. The main aim of this temperature profile was to achieve a large isothermal zone in which the active catalyst would be placed. Adjustments to the set point temperature were achieved through trial and error. Using the heating block set points in table A.1, a large 20 cm isothermal zone was achieved at a temperature of 236.5 °C. The reactor isothermal zone was determined to have an experimental error of 2 °C calculated based on the manufactures specifications. (i.e. 0.20% of the full scale 1000 °C temperature range for K-type thermocouples used with this controller). The full temperature profiles for each reactor can be found in figures A.1 and A.2 on page 55. The average individual isothermal zone temperatures can be seen in table A.2.

Using the set points in table A.1 as a basis, the temperature set points of the heating blocks could be adjusted for the desired reactor temperature. The following equation was used to determine the temperature set points of the individual blocks

$$Block\,i(^{\circ}C) = \frac{T_R\,(^{\circ}C)}{T_{R,basis}\,(^{\circ}C)} \times Block\,i_{basis}\,(^{\circ}C)\;for\;i = 1,2,3,4 \tag{A.1}$$

where $Block\,i$ is the new temperature set point for the individual block, T_R is the desired reactor temperature, $T_{R,basis}$ is the reactor temperature basis (i.e. 236.5 °C) and $Block\,i_{basis}$ is the individual heating block basis set point.

The temperature controller used for blocks 1, 2 and 3 were Gefran 800P controllers, thus meaning that temperature calculated needed to be rounded to the nearest 1 °C. The temperature controller used for heating block 4 is a Gefram 600 which allowed for the set point to be rounded to the nearest 0.1 °C. Using the equation A.1 the set point temperature for heating block 1 for a desired reactor temperature of 225°C, is 201°C. The corresponding set point temperatures for heating blocks 2, 3 and 4 are 199 °C, 196 °C and 197.9 °C respectively.

The isothermal zone temperature profile was then retested and found to be marginally lower than the desired temperature. It was found that the energy introduced through friction by moving the thermocouple inside the thermowell had resulted in an increased basis set point of approximately

2 °C at each point in the reactor (thus not affecting the size of the isothermal zone but only the accuracy of the measured temperature). A new temperature profile was then done allowing for any frictional heating to dissipate and the set points readjusted to give the desired reactor isothermal zone temperature of 225°C. These set points can be seen in A.3 and were used as the basis set points throughout the experiment.

Table A.1: Heating block set point temperatures used to determine isothermal reactor zone.

Reactor Temperature	236.5 °C
Heating Block 1 (top) Set Point	211 °C
Heating Block 2 Set Point	209 °C
Heating Block 3 Set Point	206 °C
Heating Block 4 (bottom)	208 °C

Table A.2: Individual reactor isothermal temperatures.

Reactor 1 (Left Reactor)	236.7 °C
Reactor 2 (Right Reactor)	236.4 °C
Average Measured Temperature	236.5 °C
Error	2 °C

Table A.3: Heating block set points for a desired reactor temperature of 225 °C

Reactor Temperature	225 °C
Heating Block 1 (top) Set Point	202 °C
Heating Block 2 Set Point	201 °C
Heating Block 3 Set Point	197 °C
Heating Block 4 (bottom)	199.6 °C

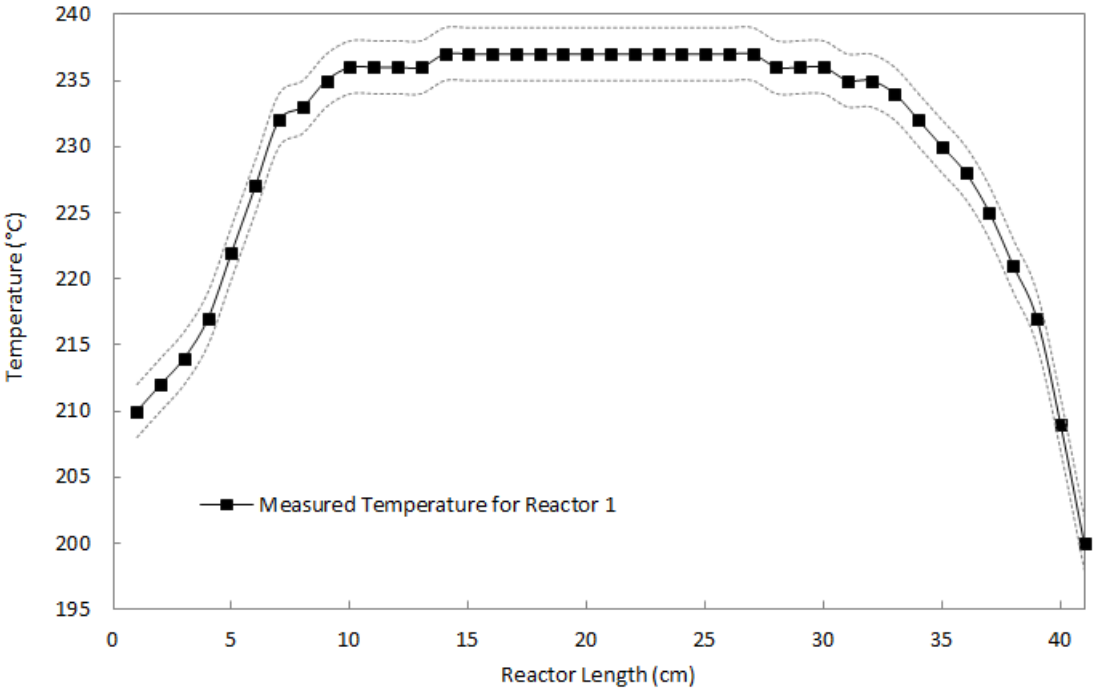

Figure A.1: Reactor 1 isothermal temperature zone with error band.

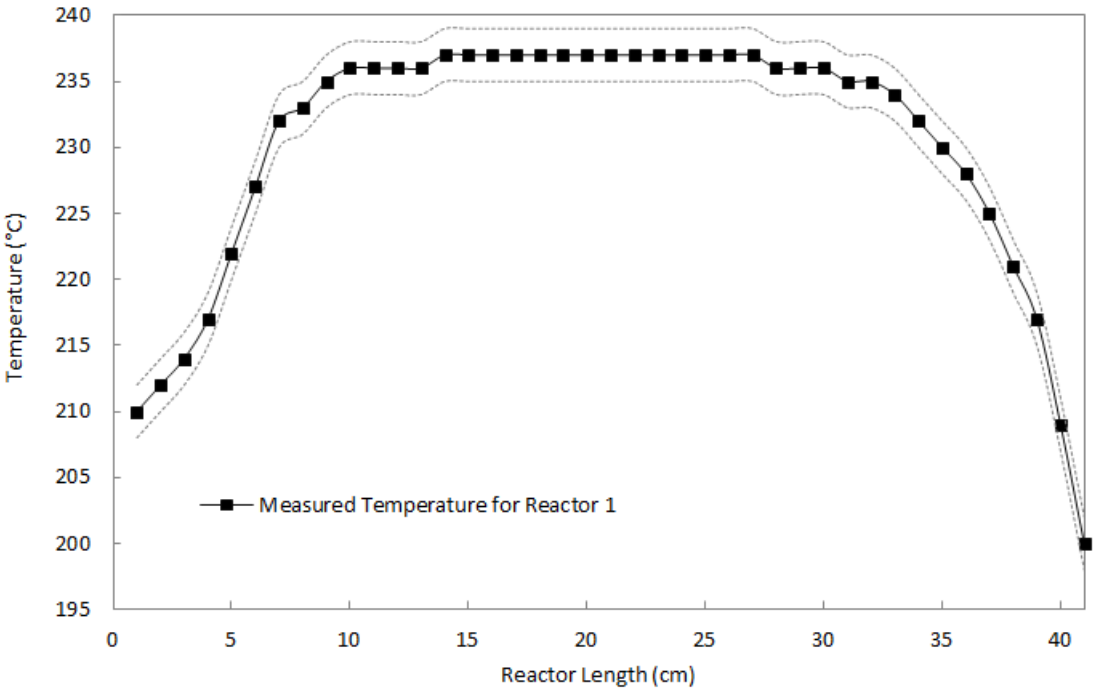

Figure A.2: Reactor 2 isothermal temperature zone with error band.

Appendix B
Nitrogen Dilution

The nitrogen dilution flow rate was determined by calibration of the pressure regulators supplying the nitrogen gas to the vaporizer. To ensure complete vaporization of the reactor products a nitrogen flow rate of 200 ml/min is required to mix with the reactor products.

Flow Analysis and Pressure Effects

For flow of gas through the capillary in reactors the combined effect of excess friction (as a result of capillary length) and flow constriction resulted in the phenomenon known as choked flow at inlet pressures above 38 bar (seen in reactor 1). Choked flow occurs when the linear gas velocity exceeds the speed of sound. This caused the dilution rate to remain constant even with increasing the inlet capillary pressure.

Under normal flow conditions the venturi effect illustrates that as the gas is constricted the linear gas velocity increase preserving the conservation of mass. This in turn results in a decrease in pressure as to conserve mechanical energy. Along the length of the capillary tube the friction factor is governed by the resistance parameter N shown below in equation B.1 (Green et al., 2008):

$$N = \frac{4fL}{D_H} \tag{B.1}$$

where f is the fanning friction factor, L is the length of the tube and D_H is the hydraulic diameter. The equation shows that the resistance parameter is directly proportional to the length of the tube. The force exerted by the capillary walls along the length of the tube reduce the pressure further increasing the velocity of the gas until choking occurs. The effect of the different capillary tube lengths on the different reactors (and thus the pressure loss) can be seen in the calibration equation gradient (i.e. reactor 2 capillary is shorter therefore the gradient is less steep as a result of a lower pressure drop due to friction).

Using the equations in (Green et al., 2008) the approximate critical pressure ratio can be calculated.

$$\frac{p_*}{p_0} = \left(\frac{2}{k+1}\right)^{\frac{k}{k+1}} = 0.527 \tag{B.2}$$

where $\frac{p_*}{p_0}$ is the critical pressure ratio (downstream/upstream) and k is the specific heat ratio for N_2 (equal to 1.4). This indicates that increasing the dilution upstream pressure above approximately 38 bar should not result in an increase in the dilution flow rate. This was evident in the calibration of reactor 1 as an increase in upstream pressure above 40 bar did not increase the dilution flow rate.

As a dilution flow rate of 250 ml/min is desired, the option of shortening the capillary tube in reactor 1 was assessed in order to reduce the pressure loss by friction. This was however not carried out due to the brittle nature of the capillary tubes and the risk of damage to the tube upon removal from the rig. A dilution flow rate of 200 ml/min was thus used as a compromise.

Nitrogen Dilution Rate

The calibration graphs for the nitrogen dilution flow rate pressure regulator set points can be seen in figures B.1 and B.2. Using these graphs and a dilution rate of 200 ml/min, the pressure regulators were set to 38 bar for reactor 1 and 40 bar for reactor 2. These settings remained unaltered throughout all the experiments conducted.

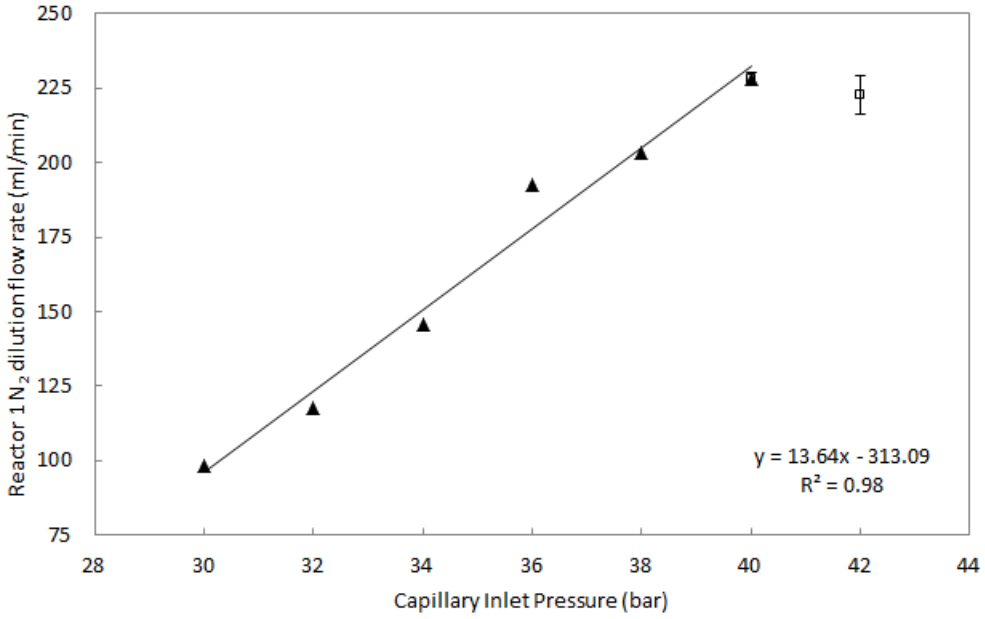

Figure B.1: Reactor 1 N_2 dilution flow rate inlet capillary pressure calibration graph.

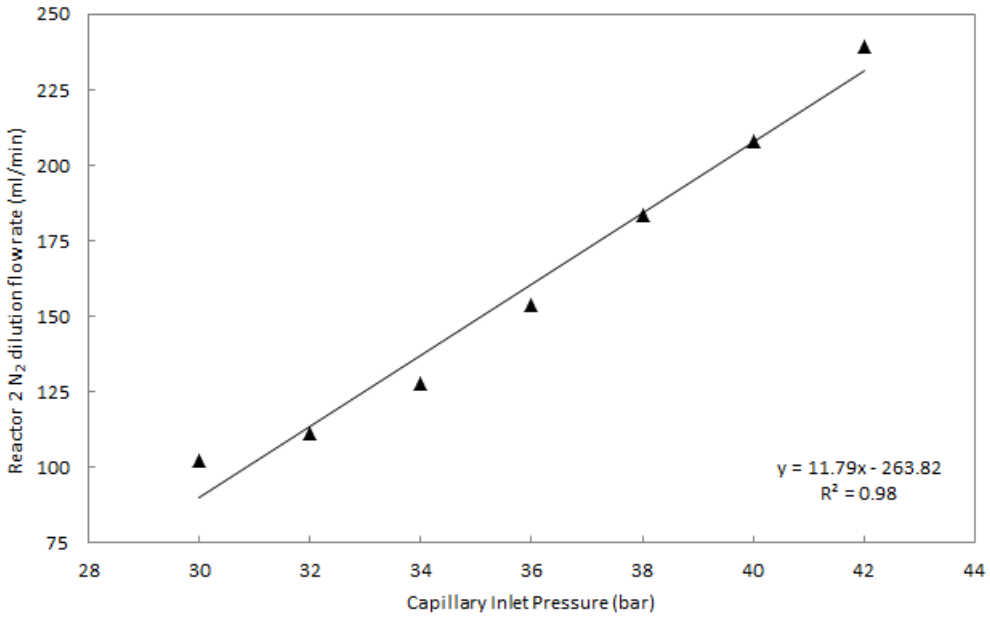

Figure B.2: Reactor 1 N_2 dilution flow rate inlet capillary pressure calibration graph.